

# The 4th IBIS/ISGRI soft gamma-ray survey catalog<sup>1</sup>

A. J. Bird<sup>1</sup>, A. Bazzano<sup>2</sup>, L. Bassani<sup>3</sup>, F. Capitanio<sup>2</sup>, M. Fiocchi<sup>2</sup>, A. B. Hill<sup>1,4</sup>, A. Malizia<sup>3</sup>, V. A. McBride<sup>1</sup>, S. Scaringi<sup>1</sup>, V. Sguera<sup>3</sup>, J. B. Stephen<sup>3</sup>, P. Ubertini<sup>2</sup>, A. J. Dean<sup>1</sup>, F. Lebrun<sup>5,6</sup>, R. Terrier<sup>5</sup>, M. Renaud<sup>5</sup>, F. Mattana<sup>5</sup>, D. Gotz<sup>6</sup>, J. Rodriguez<sup>6</sup>, G. Belanger<sup>7,5</sup>, R. Walter<sup>8</sup>, C. Winkler<sup>9</sup>

## ABSTRACT

In this paper we report on the fourth soft gamma-ray source catalog obtained with the IBIS gamma-ray imager on board the *INTEGRAL* satellite. The scientific dataset is based on more than 70 Ms of high quality observations performed during the first five and a half years of Core Program and public observations. Compared to previous IBIS surveys, this catalog includes a substantially increased coverage of extragalactic fields, and comprises more than 700 high-energy sources detected in the energy range 17–100 keV, including both transients and faint persistent objects which can only be revealed with longer exposure times. A comparison is provided with the latest *Swift*/BAT survey results.

*Subject headings:* gamma-rays: observations, surveys, Galaxy:general

## 1. Introduction

Since its launch in 2002, the *INTEGRAL* (International Gamma-Ray Astrophysics Laboratory) observatory has carried out more than 7 years of observations in the energy range from 5 keV

<sup>1</sup>School of Physics and Astronomy, University of Southampton, SO17 1BJ, UK

<sup>2</sup>IASF/INAF, Rome, Italy

<sup>3</sup>IASF/INAF, Bologna, Italy

<sup>4</sup>Laboratoire d’Astrophysique de Grenoble, UMR 5571 CNRS, Université Joseph Fourier, BP 53, 38041 Grenoble, France

<sup>5</sup>AstroParticule et Cosmologie (APC), CNRS-UMR 7164, Université Paris VII, Paris, France

<sup>6</sup>CEA Saclay, DSM/Irfu/Service d’Astrophysique, F-91191, Gif-sur-Yvette, France

<sup>7</sup>ESA/ESAC, PO Box 78, 28691 Villanueva de la Canada, Spain

<sup>8</sup>ISDC, Geneva Observatory, University of Geneva, Chemin d’Ecogia 16, 1291 Versoix, Switzerland

<sup>9</sup>ESA-ESTEC, Research and Scientific Support Dept., Keplerlaan 1, 2201 AZ, Noordwijk, The Netherlands

<sup>1</sup>Based on observations with INTEGRAL, an ESA project with instruments and science data centre funded by ESA member states (especially the PI countries: Denmark, France, Germany, Italy, Switzerland, Spain), Czech Republic and Poland, and with the participation of Russia and the USA.

– 10 MeV. *INTEGRAL* is an observatory-type mission, and most of the total observing time (65% in the nominal phase, 75% during the mission extension) is awarded as the General Programme to the scientific community at large. Typical observations last from 100 ks up to two weeks. As a return to the international scientific collaborations and individual scientists who contributed to the development, design and procurement of *INTEGRAL*, a part of the observing time (from 35% to 25%) was allocated to the Core Programme. During the nominal lifetime (5 years) this programme consisted of three elements, a deep exposure of the Galactic central radian, regular scans of the Galactic Plane, pointed observations of the Vela region and Target of Opportunity follow-up. In order to exploit *INTEGRAL*'s unique capabilities, *Key Programmes* were introduced in 2006 (AO5). These are deep observations requesting a few Ms observing time that allow the observatory to accommodate various different requests of the community at large by amalgamating many individual scientific targets present in the selected sky fields as well as ultra-long nucleosynthesis and diffuse emission studies.

The IBIS (Imager on Board *INTEGRAL* spacecraft) imaging instrument is optimised for survey work with a large ( $30^\circ$ ) field of view with excellent imaging and spectroscopy capability. Instrumental details and sensitivity can be found in Ubertini et al. (2003). The data are collected with the low-energy array, ISGRI (*INTEGRAL* Soft Gamma-Ray Imager; Lebrun et al. (2003)), consisting of a pixellated 128x128 CdTe solid-state detector that views the sky through a coded aperture mask. IBIS/ISGRI generates images of the sky with a  $12'$  (FWHM) resolution and typical source location of better than  $1'$  over a  $\sim 19^\circ$ (FWHM) field of view in the energy range 17–1000 keV.

A sequence of IBIS survey catalogs have been published at regular intervals as more data have become available (Table 1). The frequent Galactic Plane Scans (GPS) within the Core Programme, performed in the first year of operations, were successfully exploited to yield a first survey of the galactic plane to a depth of  $\sim 1\text{mCrab}$  in the central radian (Bird et al. 2004). This gave evidence of a soft gamma-ray sky populated with more than 120 sources, including a substantial fraction of previously unseen sources. The second IBIS/ISGRI catalog (Bird et al. 2006) used a greatly increased dataset (of  $\sim 10\text{Ms}$ ) to unveil a soft gamma-ray sky comprising 209 sources, again with a substantial component ( $\sim 25\%$ ) of new and unidentified sources. The third IBIS/ISGRI catalog (Bird et al. 2007) further increased the dataset, with a substantial improvement in extragalactic coverage, resulting in the detection of a total of 421 sources.

In this paper we provide the fourth IBIS/ISGRI soft gamma-ray survey catalog, that now comprises more than 700 high-energy sources. This fourth catalog continues to build on the source data provided by previous catalogs by incorporating an additional 2 years of data, and using the latest software and source detection techniques. Particular care has been taken to optimise the detection of the transient sources that are common in the hard X-ray sky but are only visible for a small fraction of the total exposure now available.

Table 1: Summary of the IBIS survey catalogs so far

Cat	Exposure	Dates	Sources
1	5 Ms	Feb 03 – Oct 03	120
2	10 Ms	Feb 03 – June 04	209
3	40 Ms	Feb 03 – Apr 06	421
4	70 Ms	Feb 03 – Apr 08	723

## 2. Data analysis and catalog construction

### 2.1. Input dataset and pipeline processing

The survey input dataset consists of all available pointings at the end of April 2008. This consists of the first 5 years of Core Programme observations, including the Galactic Plane Scans (GPS), Galactic Center Deep Exposure (GCDE) and all available pointed observations. Data coverage from revolution 12 (first light, November 2002) to revolution 530 (April 2007) is almost complete, while data between April 2007 and April 2008 constitute only Core Programme and public pointings. *INTEGRAL*/IBIS data is organised in short pointings (science windows, scw) of  $\sim$ 2000s. In total, 41588 science windows were input into the pipeline processing. After removal of pointings flagged as Bad Time Intervals (BTI) by the Science Data Centre (Courvoisier et al. 2003) this number is reduced to 39548 science windows of good quality data.

Pipeline processing was carried out using the standard *OSA 7.0* software (Goldwurm et al. 2003) up to and including the production of sky images for individual science windows with  $4.8'$  pixels. Five primary energy bands (20–40, 30–60, 20–100, 17–30, 18–60 keV) were used to maximise detection sensitivity for sources with various energy spectra. The input catalog used for image processing was those sources marked as detected by ISGRI in the ISDC Reference Catalog version 28, which had been updated to include all sources previously detected by the surveys and in guest observer pointings.

The overall sky exposure is summarised in Figure 1. When discussing exposure, we use the accumulated instrument livetime, corrected for off-axis coding fraction, but not corrected for energy-dependent on-axis absorption. It can be seen that near the Galactic plane, half the sky is covered with more than 1Ms of exposure, while for the whole sky, that fraction drops to  $\sim$ 15%. 90% of the sky is exposed at the 100ks or greater level. The exposure does not result from any specific pointing or operational constraints, but is merely the summation of all science observations performed during the accumulation of the dataset. The overall exposure uniformity is improving as the mission continues, and as the science program includes a greater number and diversity of targets.

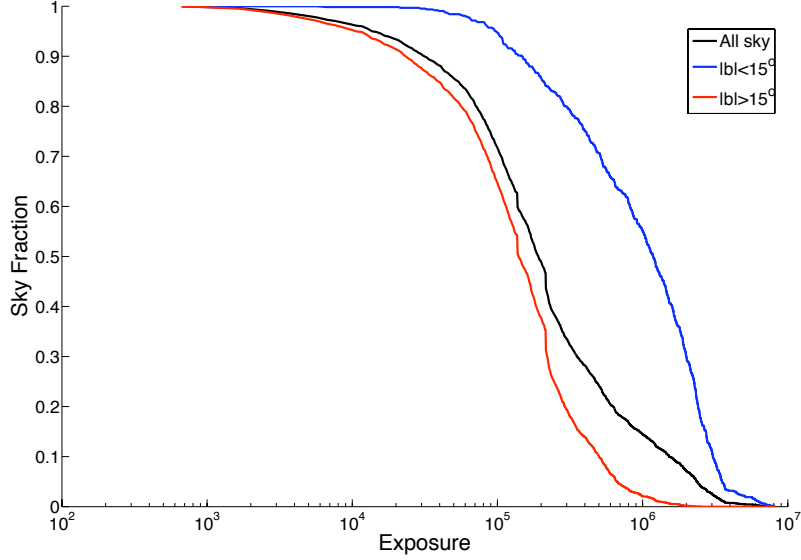


Fig. 1.— Fractional exposure as function of sky area.

## 2.2. Mosaic construction

Each scw image was tagged with its rms (after removal of sources) to act as an indicator of overall image quality. As in previous survey construction, the primary aim of this step is to remove data taken during periods of enhanced background (during solar activity or soon after perigee passage). Filtering was applied based on the rms value of the image, such that the rms should not exceed a limit of  $2\sigma$  above the mean image rms for the whole dataset). This function now somewhat overlaps with the BTI flagging provided by the ISDC, but we still remove around 5% of the science windows that exceed this rms limit. Although they are still processed, data taken in staring mode are not used in the construction of the final sky mosaic images as they contribute a far higher level of systematic noise than the standard dithered observations. Some 1230 science windows in the input dataset were flagged as consisting of staring data.

After removal of high-rms and staring data, approximately 36000 scw remained in the dataset, with a total exposure of  $\sim 70$  Ms. The selected science windows were mosaicked using a proprietary tool optimised to create all-sky galactic maps based on large numbers of input science windows. Mosaics were constructed for five energy bands (see Section 2.1), four map projections, and four timescales, all with  $2.4'$  pixel resolution, significantly oversampling the intrinsic system PSF.

We constructed mosaics over the same three timescales used for the third catalog, and a newly introduced one for identifying transients as explained in section 2.4. Maps were created for each revolution (a satellite orbit; approximately 3 days) which contained valid data. This is optimised

to detect sources active on timescales of the order of a day. We also identified 32 sequences of consecutive revolutions which had similar pointings. Thus these *revolution sequences* could best be analysed as a single observation, and sensitivity for sources on longer timescales than revolutions (i.e. order of weeks) could be optimised. Ultimately, persistent sources can best be detected in an *all-archive* accumulation of all available high-quality data. The problem of higher exposure and long timebase spanned by this latest dataset has further worsened the problem noted in the third catalog - namely that the source search methods we employ are optimised for detection of persistent flux from a source; a highly variable source may be clearly detectable during outburst, while having an undetectably low mean flux over the full dataset. In addition, we searched for the optimum detection timescale (from 0.5 days to the length of the dataset) for known or suspected sources (see section 2.4) and created one additional mosaic for each source on the optimum timescale for that source.

For each energy band and time period, all-sky mosaics were made in four projections: centred on the Galactic Center, centred on the Galactic anti-center, north galactic polar and south galactic polar. The purpose of these multiple projections is to present the automatic source detection algorithms with source PSFs with the minimum possible distortions.

### 2.3. Source searching and candidate list production

In total over 11500 maps were created at this stage of processing. Each of the mosaics was searched using two methods:

- (i) the *SExtractor 2.5* software (Bertin & Arnouts 1996). The source positions measured by *SExtractor* represent the centroid of the source calculated by taking the first order moments of the source profile (referred to by *SExtractor* as the barycenter method). Source detectability is limited at the faintest levels by background noise and can be improved by the application of a linear filtering of the data. In addition, source confusion in crowded fields can be minimised by the application of a bandpass filter. To this end, the *mexhat* bandpass filter is used in the *SExtractor* software. The convolution of the filter with the mosaic alters the source significances, hence *SExtractor* uses the source positions identified from the filtered mosaic to extract the source significances from the original mosaic.
- (ii) a proprietary ‘peakfind’ tool which employs a basic iterative removal of sources technique, combined with an assessment of the local background rms to reduce the false detection of sources in areas of the map with high systematic noise structures - mainly in crowded regions and around the brightest sources.

A list of candidate sources was constructed by merging the  $> 4\sigma$  excess lists from each mosaic, using a merge radius of 0.1 degrees. A source had to be detected by both search methods in

order to be included in the candidate list. Manual inspection was performed on each map to check for the (rare) occasions where *SExtractor* fails due to the close proximity of two sources, and any additional sources found were added to the excess list. We also added all previous declared *INTEGRAL* detections which were not detected in any of our maps, in order to be able to search for them on different timescales in the later analysis (see section 2.4).

This resulted in a list of 1266 excesses which were passed to the next stage of analysis.

#### 2.4. Light curve generation and search on all timescales

The main change initiated in this catalog compared to previous ones is intended to address the detection of variable sources. The hard X-ray sky is extremely variable, and this leads to problems in detecting sources when the search is only performed on a limited number of timescales. As an example, a source in outburst in the early mission becomes of lower and lower significance as more and more data is acquired when the source is in quiescence.

These variability issues have led to a number of unfortunate effects:

- (1) sources detected in earlier catalogs may drop below the detection threshold after long periods of quiescence.
- (2) a number of sources known to be detectable in IBIS have not been included because the source search was not optimised for the particular timescale on which the source was active.

In this catalog, we have performed a systematic search for any source detected in a previous IBIS catalog or declared as a new IBIS detection in the literature prior to April 2008 when the dataset was frozen. This was performed by creating a light curve for each source in the 18-60 keV band on science window timescales, and then scanning a variable-sized time window along each light curve. The window length is varied from 0.5 days ( $\sim 10$  scw) to the full length of the light curve, and all data points within the time window are included in the analysis. The duration and time interval over which the source significance is maximised is recorded. We define the *bursticity* of a source as the ratio of the maximum significance on any timescale, compared to the significance defined for the whole dataset. Thus a bursticity of 1 defines a persistent source, where the inclusion of any data maintains or increases the detection significance. Conversely, a bursticity of greater than 1 implies that the significance of a source can be increased by the omission of some observations from the analysis, presumably when the source was in quiescence. Note that we only use the single time interval when the significance is maximised, we do not combine multiple non-consecutive outbursts which, for some sources, could yield an even higher significance.

The impact of this bursticity analysis is significant. Around 100 sources are recovered that would not have been without this analysis. Furthermore, by defining the time interval over which the significance is maximised for every source, we gain an insight into the variability behaviour of the sources. Finally, by building a mosaic map only for the timescale of maximum significance, we

can optimise the chance of source detection and determination of some source parameters - notably the best possible source position (since error radius is inversely proportional to significance).

A few examples can serve to illustrate the effect of the bursticity analysis. The first is IGR J00245+6251, a GRB reported in the third IBIS/ISGRI catalog as an  $11.5\sigma$  detection in revolution 266. The bursticity analysis instead identifies that the source was active on a 0.5 day timescale (this is actually the minimum search time, and is still much longer than the burst itself). By mapping on a more appropriate timescale, the significance is increased to 28.6 sigma and the position error reduced from  $2.3'$  to  $1.1'$ . It should be noted that the majority of GRB and a number of other fast (duration  $< 0.5$  days) transient objects with lower fluxes are still not recovered with sufficient significance to be included in this catalog. The second is IGR J17191-2821, a transient discovered during the Galactic Bulge monitoring (Kuulkers et al. 2007). This source was therefore added to the checklist as a previously declared *INTEGRAL* detection, despite the fact that it was totally undetectable (below  $4\sigma$ ) in any of the long-term maps. It would not have been detected using the methods employed for the third catalog. Bursticity analysis, however, confirms its detection at the  $8\sigma$  level during a 1.2 day outburst. These two examples show the efficiency of finding short outbursts. However, there is another class of detection - non-persistent sources of long duration that are too faint to appear at either revolution or whole-archive timescales. Illustrating this is IGR J13400-6429, a source put forward for further analysis due to a marginal detection ( $4.0 < \sigma < 4.5$ ) in the whole-dataset maps. Mapping over the optimum 500-day period identified by bursticity analysis provides a clear  $7.5\sigma$  detection, but again this source would not have been found by the methods used for the third catalog.

At the end of this process, the significance of each source in each energy band, and for both whole dataset and ‘outburst’ are known, and these significances are used in a final decision on the acceptance of each source. An indication of the bursticity level, the significance obtained, and a peak flux during the detected outburst are included in the source list (Table 3).

## 2.5. Source list final filtering

We have performed a number of steps to minimise the possibility of false catalog entries. These methods are designed to counter both statistical fluctuations in the maps (which we can to some extent assess) and systematic effects present in the maps, which are much harder to quantify.

First and foremost, each source is manually inspected by a number of people experienced with working with IBIS/ISGRI maps. The inspection covers aspects such as PSF shape, consistency across multiple energy bands, and the significance of the source relative to the *local* noise levels in the map. We require a unanimous agreement among many viewers that the excess is a true source, a very conservative approach, but one designed to minimise the false detection rate.

A flux-exposure analysis has been carried out in which each detected flux has been compared to the predicted minimum detectable flux for the exposure in which the detection was made.

Sources for which the mean flux is much lower than that which could reasonably be detected in a corresponding timescale may have been boosted by systematic effects, or may just be an outlier in the statistical fluctuations of the maps - in either case, the excess is rejected.

## 2.6. Detection Significance thresholds

In order to identify an excess in one of the mosaicked images it is necessary to determine the significance level at which the source population dominates over the noise distribution. To this end we produce a histogram of the individual pixel significance values in each of the mosaics where a source was found. A Gaussian, with mean  $\sim 0$  and standard deviation  $\sim 1$ , is a found to be a good representation of the noise distribution. This is shown in Figure 2 for the 18–60 keV all-sky mosaic; at high significances it is clear the data deviates from the noise distribution model.

Looking at the pixel significance distribution across all mosaics we can confidently conclude that  $<<1\%$  of the pixels found at significances above  $4.8\sigma$  are produced by the statistical noise distribution. Furthermore, in the 18–60 keV all-sky mosaic, of the pixels found between  $4.5$ – $4.8\sigma$   $<6\%$  are from the statistical noise distribution. However, these limits are based upon the global properties of the mosaics and the maps contain systematic errors which are localised to specific regions. The majority of the systematic noise is produced from the very brightest sources and from very crowded regions. This is dealt with through the visual inspection of each candidate excess in the context of the region of sky in which it has been detected.

## 3. Galactic Center Localizations

The Galactic Center region poses a number of specific problems for the determination of the source population which gives rise to the emission seen by IBIS/ISGRI. A number of the sources there are not fully spatially resolved and are highly variable, and the region is subject to some systematic structures which make the identification of faint sources difficult.

A  $50.4' \times 52.8'$  image in the 20–40 keV band centred at  $l = 0.12^\circ$ ,  $b = 0.18^\circ$  was extracted from each revolution during which the Galactic Center was observed ( $\sim 140$  in total). The region was optimised to minimise the impact of nearby known bright sources but to allow good assessment of the local background statistics. A core set of three sources, 1E 1743.1–2843, SAX J1747.0–2853 and IGR J17456–2901, was used as a starting point, the evidence of their presence being determined from simultaneous, spatially well-separated detection with JEM-X during observations of the Galactic Center and Bulge region performed in revolutions 407–429 (Feb – April 2007).

For each revolution these three sources were fit as two-dimensional Gaussians with their positions fixed to those in Kuulkers et al. (2007), FWHM fixed to 5 pixels (the PSF of the mosaics described above) and normalisations free to vary. The Gaussian can be taken as an adequate ap-

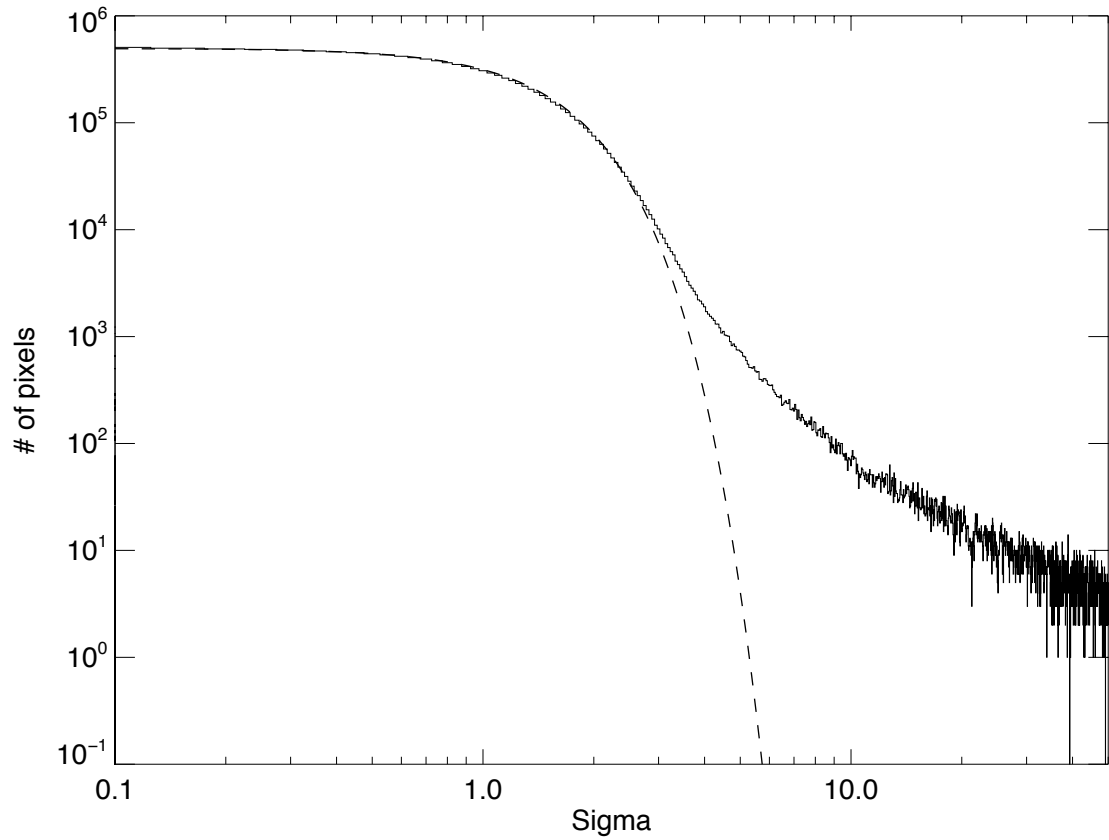


Fig. 2.— Distribution of individual pixel significances found in the 18–60 keV all-sky mosaic. The solid line represents the data; the dashed line represents a Gaussian fit to the noise distribution.

proximation of the true PSF (Gros et al. 2003) given that the images are typically constructed from  $\sim 50$  dithered science windows. If  $\chi^2_\nu >> 1$ , and a significant ( $> 3\sigma$ ) excess was present in the residuals, a new Gaussian was added with both position and normalisation free to vary. The presence of bright sources centered outside of the fitting region, but still influencing it, was taken into account when necessary. The procedure was repeated for the ‘North Blend’, a region centered at  $l = -0.08^\circ$ ,  $b = 1.38^\circ$ . The two fitting regions are shown in Figure 3.

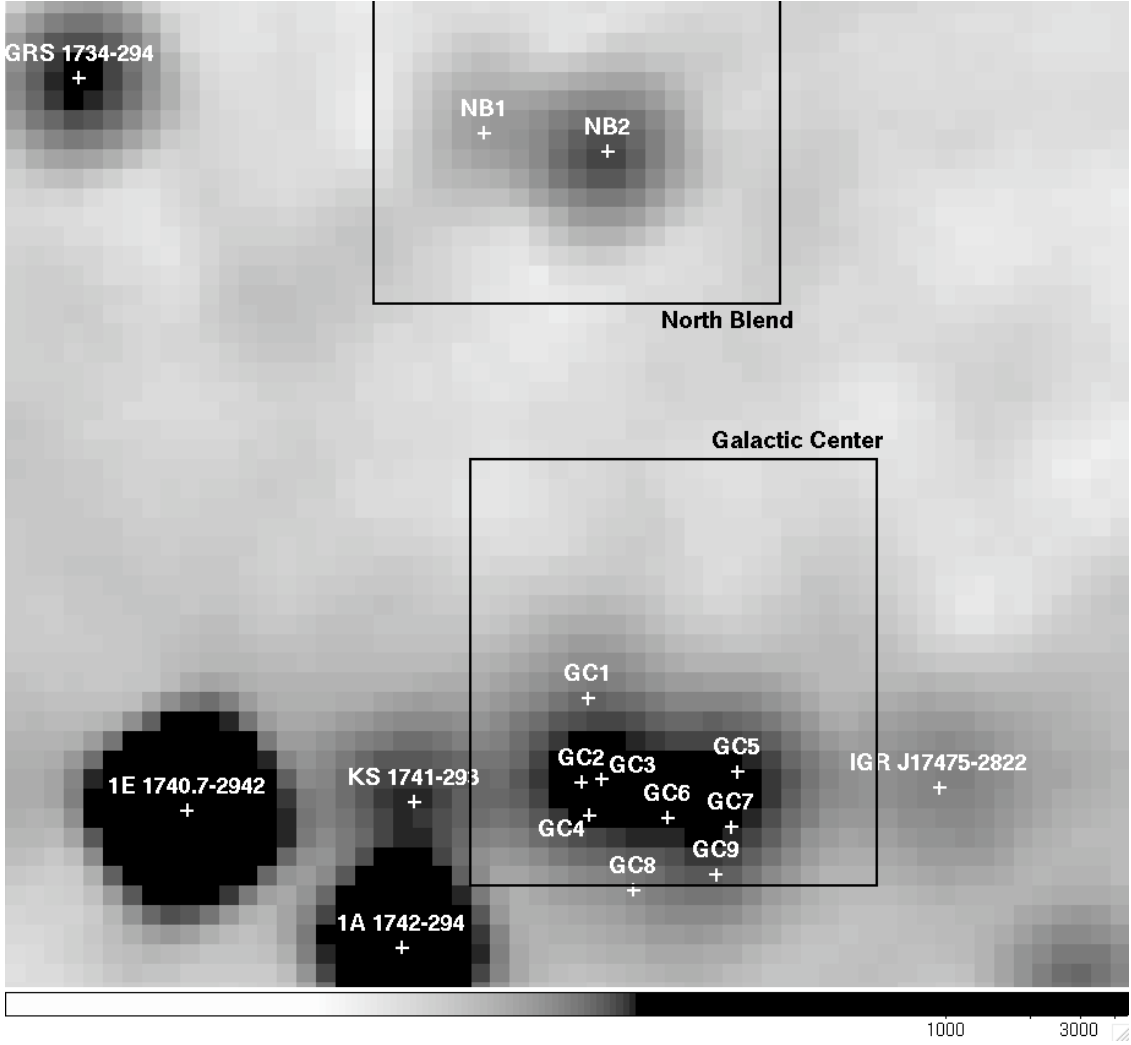


Fig. 3.— Fitting regions and resulting sources for analysis of Galactic Center and North Blend.

The fit results from all revolutions were merged and a consistent set of nine sources in the Galactic Center and two in the North Blend was generated. All sources resulting from these fits are identified as B1GCF in the mapcode column of the source list and shown in Table 2. Apart from the three core sources listed above, we confirm the detection of GRS 1741.9–2853 and detect five new variable sources. The limited angular resolution of IBIS prevents these from being unambiguously

associated with previous X-ray sources. The time variability and nature of these sources will be discussed in more detail in a future publication.

Table 2: Sources required in Galactic Centre and North Blend fitting

ID	Name	R.A.	Dec.	New
NB1	XTE J1739–285	264.989	-28.487	N
NB2	SLX 1737–282	265.179	-28.291	N
GC1	GRS 1741.9–2853	266.249	-28.919	N
GC2	IGR J17456–2901	266.410	-29.021	N
GC3	IGR J17457–2858	266.428	-28.982	Y
GC4	IGR J17459–2902	266.485	-29.043	Y
GC5	1E 1743.1–2843	266.580	-28.735	N
GC6	IGR J17463–2854	266.587	-28.907	Y
GC7	IGR J17467–2848	266.683	-28.805	Y
GC8	IGR J17468–2902	266.690	-29.045	Y
GC9	SAX J1747.0–2853	266.761	-28.883	N

#### 4. The Table Data

The name of the source is given following the convention to quote wherever possible the name declared at the time of the first X-ray detection. The names are given in bold for the  $\sim 300$  sources added to the catalog since the third catalog.

The astrometric coordinates of the source positions were extracted from the mosaics by the barycentring routines built into *SExtractor 2.5*. In almost all cases, the position for a source was extracted from the map yielding the highest source significance. In a few cases, primarily for blended sources, other maps were chosen in order to minimise the interference of other sources. Simultaneous fitting of multiple Gaussian PSFs was used in the most difficult cases - these sources are indicated as blended in the notes accompanying the table. The point source location error of IBIS is highly dependent upon the significance of the source detected (Gros et al. 2003). We use this formulation, combined with the significance of the detection used to locate the source, in order to define an error on the source position. The source localisation errors quoted are for the 90% confidence limit.

The mean fluxes quoted in the table as  $F_{20-40}$  and  $F_{40-100}$  are the time-averaged fluxes over the whole dataset derived in two energy bands (20–40 and 40–100 keV). These are provided for compatibility with past catalogs, but we note that their relevance as an *average* measure diminishes as the dataset increases and becomes longer than the average time of activity for many of the sources. Therefore, in addition for variable sources, we provide a variability indicator and indicative peak flux in the 20–40 keV band. A flag of Y indicates a bursticity  $> 1.1$  (ie a 10% increase in significance can

be obtained by selecting a subset of the data. A flag of YY indicates a bursticity of  $> 4$ , indicating a strongly variable source. In both cases, the peak flux is defined as the mean flux during the single period of time for which the significance is maximised.

The type of the source is encoded into up to 4 flags, which are explained in the table footnotes. We have followed the convention of (Liu et al. 2007) wherever possible. Identifications, and hence source types, are provided only if considered robust.

The exposure quoted is the total effective exposure on the source after all filtering of the data has been carried out.

The significances quoted are the highest significance in any single map (the map from which the significance is derived is also identified in the table), since this gives the best indication of the robustness of source detection. However, it should be noted therefore that the flux and significance values may derive from different energy bands and/or subsets of the data, and may initially appear contradictory.

## 5. Discussion

We have derived an ‘unbiased’ catalog of 723 sources observed in a systematic analysis of the IBIS/ISGRI Core Programme and public data spanning nearly 5 years of operation. Of these, 684 are secure detections of greater than  $4.8\sigma$ , the remainder are detected with between 4.5 and  $4.8\sigma$  but still with a good statistical significance.

We can estimate the minimum detectable flux as a function of the sky position (Figure 4) based on the accumulated exposure. The sensitivity of the survey is still strongly biased by the non-uniform exposure. Within the region of the Galactic Plane,  $\sim 70\%$  of the sky is covered to better than 1mCrab sensitivity, while 90% of the extragalactic sky is now covered at the 5mCrab level.

The evolution of the numbers of sources through the 4 IBIS/ISGRI catalogs is shown in Figure 5 and 6. Starting with the first IBIS survey release, we note a continuous increase in the number of extragalactic sources accounting initially for only 4% of the detected sources in 2005 and now 35% in the latest source list (see Figure 6). Experience from previous studies shows that this number will increase further once follow up of the currently unidentified sources can be initiated. It is clear that the changes in the sources dominating the catalogs are strongly linked to the sky coverage. *INTEGRAL* spent the first 4 years more on the plane and in particular in the region of the Galactic Bulge while more recently the high latitude sky has been exposed more thoroughly.

There are 331 new sources when compared to the third catalog. Of these,  $\sim 120$  are associated with extragalactic sources, while only  $\sim 25$  are associated with known Galactic sources, and the remainder are so far unidentified. This could lead us to conclude that *INTEGRAL* is now primarily detecting extragalactic objects and that the survey of the Galactic Plane has reached its limits.

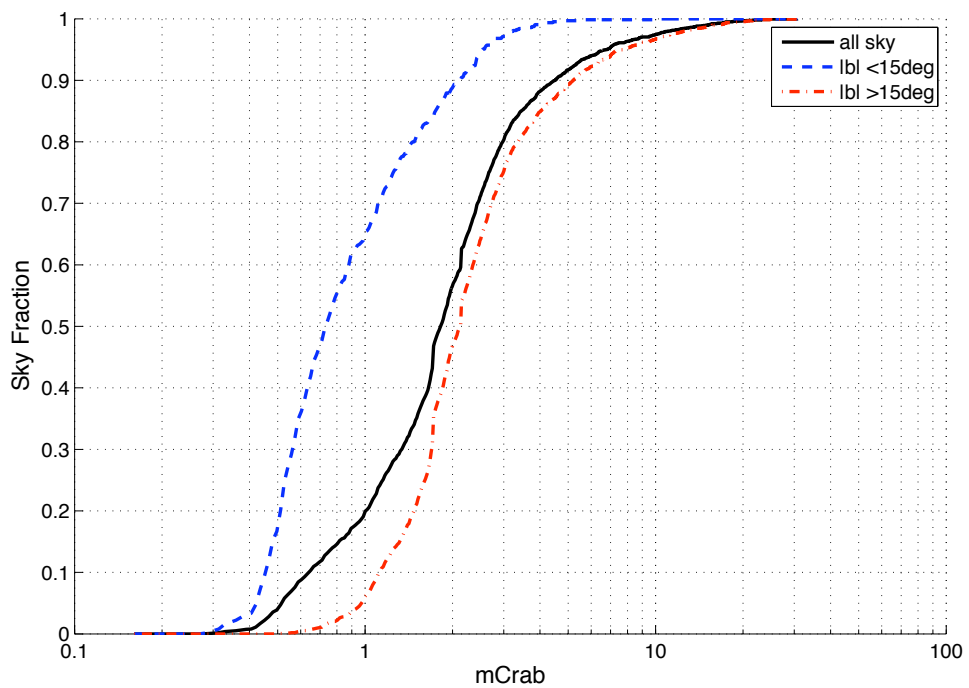


Fig. 4.— Sky fraction as function of minimum detectable flux.

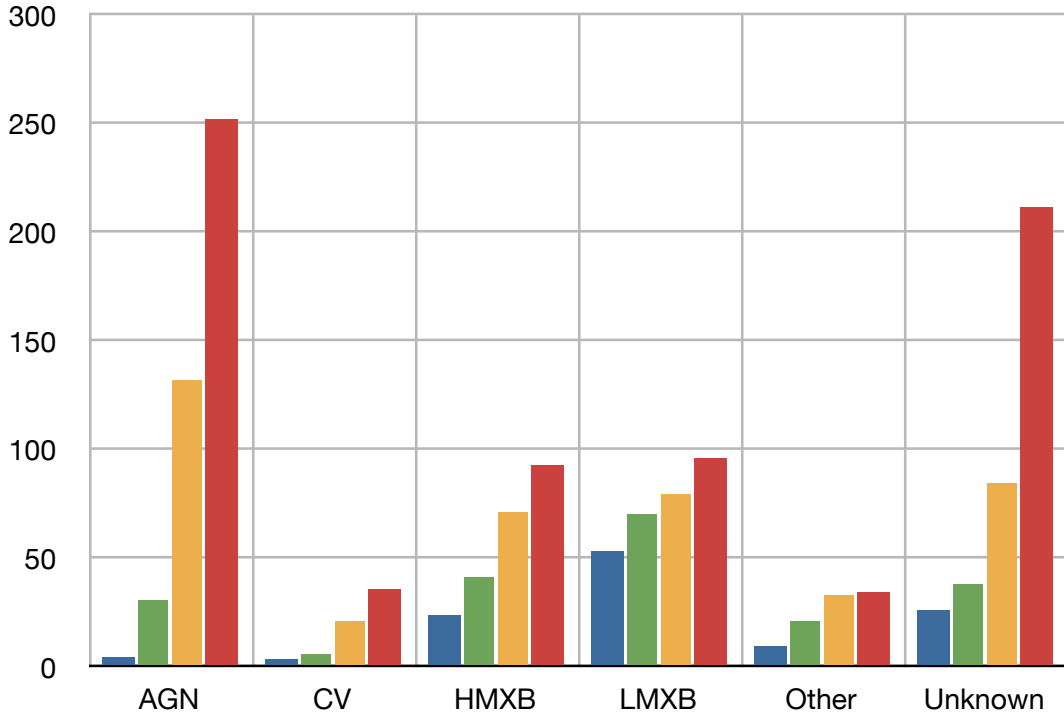


Fig. 5.— Evolution of source type and number through the 4 IBIS/ISGRI catalogs produced to date.

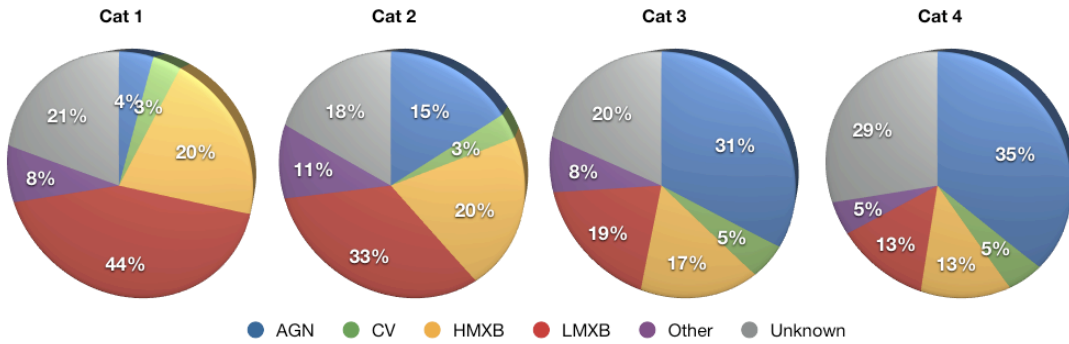


Fig. 6.— Classifications of sources in the 4 IBIS/ISGRI catalogs produced to date.

However, the sky distribution of new sources (Figure 7) shows a rather different picture. When superimposed on the delta exposure (ie the increase in exposure since the third catalog) the new sources can be seen to be following the exposure, and still comprises a very significant Galactic component. We are forced to conclude therefore, that while the extragalactic observations are at a sensitivity limit where IBIS is still re-detecting known objects, the observations near the Galactic Plane have reached a level of depth where previous X-ray observations are no longer always able to provide associations for the new sources. Combined with the variability of the Galactic sources, this is a clear indication that further observations of the Galaxy will continue to uncover new sources, and follow-up of these new sources is of critical importance. However, we should also point out that many of the new sources found in the Galactic Plane by *INTEGRAL* have been identified as AGN, so this separation of Galactic and extra-galactic sources is not a straightforward one.

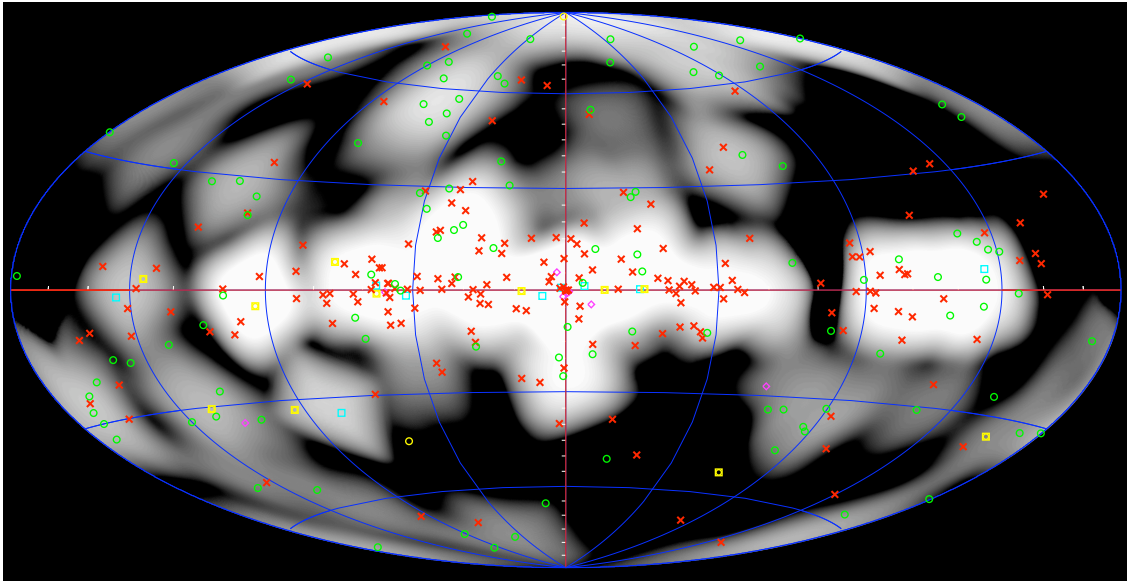


Fig. 7.— Map of incremental exposure since the third catalog, showing the locations of the new sources found. Key: Green circles = AGN; Cyan squares = HMXB; Magenta diamonds = LMXB; Yellow boxes = CVs; Red crosses = Unknown.

With regards to the ‘unknown’ sources that now constitute nearly 30% of the source list, one of the main values of this catalog will be to provide hard X-ray sources that will need follow-up at X-ray wavelengths in order to reach a firm identification. To this end, we expect a large fraction of them to be identified in the coming year, as part of an ongoing multi-wavelength campaign. In the third IBIS catalog, 113 sources were not firmly classified. Many of these sources have been followed up at other wavelength starting with an X-ray observation to provide more precise location, allowing for more diagnostic optical or infrared observations. As a result of these observations, 24 previously unidentified sources now have a firm identification and 16 have a tentative but unconfirmed identification. The firm classifications comprise 10 AGNs, 5 CVs, 5 HMXB, 3 LMXB and an XB while tentative classifications are obtained for a further 3 new AGNs, 5 HMXB, 4 LMXB,

a CV, a PWN and 2 XBs.

Twenty nine of the sources listed in the third IBIS/ISGRI catalog are not present in this list, for a number of reasons. Three sources (ESO 328–IG036, 1RXS J133447.5+371100, MCG–02–08–014) meet all our inspection criteria but are formally below the  $4.5\sigma$  threshold for this fourth catalog. Three of the sources have been removed as part of the reanalysis of the blended regions in the Galactic Center (see section 3). Two sources are no longer detectable because of changes to the dataset (due to use of BTI filtering), and 6 more are rejected as potentially associated with structures around the Galactic Center, LMC or other bright sources. The remaining 16 sources must be considered as likely due to statistical fluctuations in the maps used for the third catalog - indeed 4 of the sources are seen to be associated with low ( $<100$ ks) exposures in that catalog. The prediction made in the third catalog was for four false sources (representing 1% of the sample) above the  $5\text{--}6\sigma$  cuts, and 10 sources (20% of the sample) below, whereas the actual numbers are 7 and 9 respectively. Thus we can conclude that the measures taken to quantify false detections from a statistical viewpoint are robust and reasonably accurate.

We also note the reappearance of one source, IGR J07506–1547, detected in the second IBIS/ISGRI catalog, but not the third. As a result of the bursticity analysis, we are able to confirm the detection of this source that was clearly more active during the early mission phase.

In this catalog, we can state that the detections about  $4.8\sigma$  are drawn from an ensemble of maps, all of which show statistical quality that indicates much less than 1% of the excesses above that level will be false detections. Of the 40 sources below  $4.8\sigma$ , half are associated with known X-ray emitters, and the estimated  $\sim 6\%$  false detection rate should result in a total number of false detections in this catalog of no more 10, with the vast majority drawn from the sources detected below  $4.8\sigma$ .

### 5.1. Comparison with other hard X-ray catalogs

It is informative to compare our source list with those coming from other surveys performed in a similar energy range with imaging instruments.

The first relevant comparison is with the *SIGMA/GRANAT* observations performed through 8 years of operational life, providing  $\sim 30$  Ms of exposure to observe one quarter of the sky, of which 9 Ms were devoted to the Galactic Center region. *SIGMA* was characterised by  $15'$  angular resolution and  $2\text{--}3'$  accuracy of source location over an energy range of 35 – 1300 keV. The sensitivity of *SIGMA* to the overall sky was about 100 mCrab reaching 8–10 mCrab for the Galactic Center region. A total of 37 objects were detected above 35 keV, of which 5 were extra-galactic, and 32 galactic, including 8 X-ray novae (Revnivtsev et al. 2004). The IBIS catalog includes all the *SIGMA* extragalactic detections, and all the Galactic ones with the exception of 5 transient neutron star systems (KS 1731–26, Tra X–1, GRS 0834–43, GRS 1227–025, GRO 1744–28) and the 8 X-ray novae. The non-detection by IBIS (so far) of these 13 transient systems can be attributed to their

long recurrence times between outbursts, together with a low quiescent flux.

Up until the advent of *INTEGRAL* and, 2 years later, *Swift*, no other imaging instruments were able to improve on the SIGMA results. But now both *INTEGRAL* and *Swift* are producing surveys of the hard X-ray sky, and a comparison between the most recent results from these missions is informative. The most recent BAT/SWIFT catalog (Cusumano et al., 2009) lists 754 sources in the range 14–150 keV derived from 962 detections above  $4.8\sigma$  in at least one of 3 energy bands (14–150, 14–30, 14–70 keV). This is based on 72.7 Ms exposure that is very similar to the IBIS one reached with this fourth catalog. The main difference between the sky as surveyed by the two instruments resides in the ratio of the Galactic and extra-galactic source populations. The IBIS sky in the range 20–100 keV is almost equally shared by Galactic (36%), extragalactic (35%) and unidentified sources (29%). Conversely, the extra-galactic sources account for 69% of the BAT list, which contains only 27% Galactic objects and 4% of sources known to be X- or gamma-ray emitters not yet identified. Within the two lists the most evident difference is the very high number of blazars from BAT of which IBIS detected only 30%. This could be explained by both the different exposure/sensitivity, larger FOV and by the flaring activity characterizing these objects. Once parts of the sky recently exposed with *INTEGRAL* via the Key Programmes are added to the existing public database, we will be in a better position to fully investigate this difference.

Cross-correlation of the IBIS and BAT source lists results in 333 correlations within  $\sim 400''$ , the number of false correlations at this level should be around 0. Figure 8 on the other hand shows the histogram of the exposure for all BAT sources seen in this IBIS catalog (solid line) and the same for all sources not seen in this IBIS catalog (dotted line). Clearly, the great majority of those not seen have a low exposure in IBIS (around 100 below 50ks seconds and another 200 below 200ks). Thus we can conclude that the majority of the differences between the two source lists can be explained by exposure, with any differences at higher exposures likely due to transient sources detected in one or other catalog.

Finally, we note that the current IBIS survey includes all sources reported by the SPI team except one, SPI J1720–49, for which no further information apart from that the source is variable is available until now (Bouchet et al. 2008). Since the usable SPI sensitivity extends to considerably higher energies than IBIS covers effectively, this implies that there are no sources emitting very hard spectra, or lines above  $\sim 200$  keV within the SPI sensitive range.

## 5.2. Concluding comments

It is interesting to note the different aim of the *INTEGRAL* and *Swift* missions that are very clearly demonstrated by the different source populations in the two catalogs. We anticipate that the large difference in the numbers of AGNs with the two lists of sources will be reduced soon once the deep exposures obtained with the *INTEGRAL* Key Programmes in AO6 become public and the new AO7 pointings are performed. The current survey shows that IBIS has sufficient sensitivity to

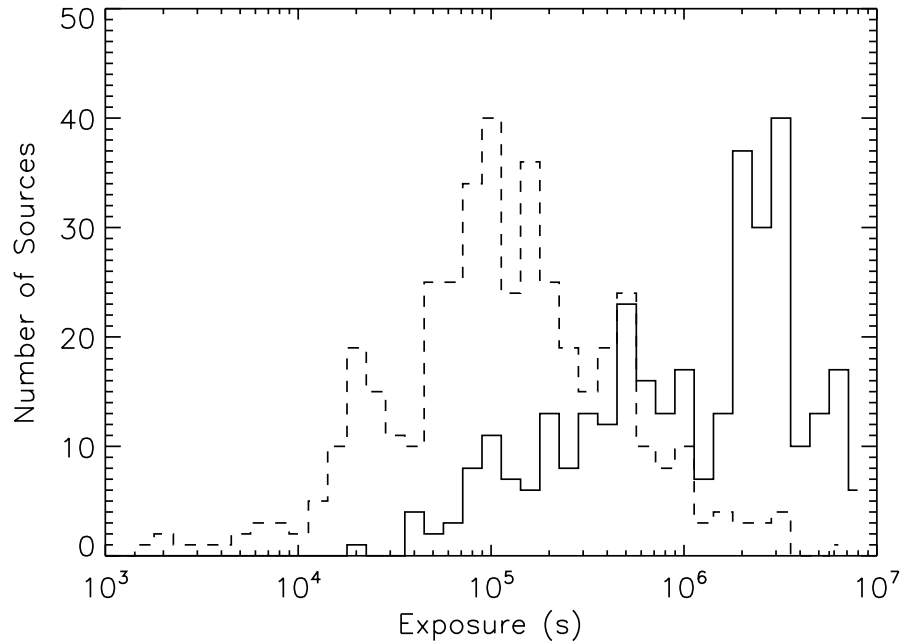


Fig. 8.— IBIS exposure for SWIFT catalogue sources. The solid line is that for those detected in this catalog whilst the dashed line is for those not detected. It is clear that the sources not detected by IBIS have in general a much shorter exposure time which will account for their not being seen. In the overlap region around  $10^5$ – $10^6$  seconds the lack of detection in IBIS can be ascribed to source strength and variability reasons.

detect weak AGNs when these exposures are carried out. Furthermore, the overall picture from the new unidentified sources, accounting for 30% of our list, indicates the existence of a large galactic population still to be discovered, and we are confident that even in this case the new deep pointings planned for next year (AO7) will result in new source discoveries, possibly new class of objects as in the case of the obscured ones. The hard X-ray sky requires dedicated observations to solve some of the critical issues currently debated such as the contribution of different types of sources to the X-ray background, the distribution of intrinsic absorption in sources, and diversity within the same class of objects. *Swift* and *INTEGRAL* have been shown to be complementary and have opened new windows of investigations. Moreover, complete and unbiased surveys are of great benefit to studies now being undertaken of the very high energy sky, acting alongside the large soft X-ray database to allow for identification and broad-band analysis of H.E.S.S, MAGIC, VERITAS, AGILE and now FERMI sources.

We acknowledge the following funding: Italian Space Agency financial and programmatic support via contracts ASI I/008/07; in UK via STFC grant ST/G004196/1; in France, we thank CNES for support during development of ISGRI and *INTEGRAL* data analysis. This research has made use of: data obtained from the High Energy Astrophysics Science Archive Research Center (HEASARC) provided by NASA's Goddard Space Flight Center; the SIMBAD database operated at CDS, Strasbourg, France; the NASA/IPAC Extragalactic Database (NED) operated by the Jet Propulsion Laboratory, California Institute of Technology, under contract with the National Aeronautics and Space Administration.

## REFERENCES

- Bertin, E. & Arnouts, S. 1996, A&AS, 117, 393  
Bird, A.J., Barlow, E.J., Bassani, L., et al. 2004, ApJ, 607, 33  
Bird, A.J., Barlow, E.J., Bassani, L., et al. 2006, A&A, 445, 869  
Bird, A.J., Malizia, A., Bazzano, A., et al. 2007, ApJS, 170, 175  
Bouchet et al., Jourdain, E., Roques, J.-P., et al. 2008, Ap J., 679, 1315  
Combi, J. A., Ribo, M., Mirabel, I. F., et al. 2004, A&A, 422, 103  
Courvoisier, T.J.L., et al. 2003, A&A, 411, L53.  
Cusumano et al., astroph-0906.4788.  
Goldwurm, A. David, P., Foschini, L., et al. 2003, A&A, 411, 223  
Gros, A., Goldwurm, A., Cadolle-Bel, M., et al. 2003, A&A, 411, L179

- Kuulkers, E., Shaw, S.E., Paizis, A., et al., 2007, A&A, 466, 595.
- Lebrun , F., Leray, J.P., Lavocat, P., et al. 2003, A&A, 411, L141
- Liu, Q.Z., van Paradijs, J., van den Heuvel, E.P.J., 2007, A&A, 469, 807.
- Monet, D. G., Levine, S. E., Canzian, B., et al. 2003, AJ, 125, 984
- Revnivtsev M.G, Sunyaev, R.A., Gilfanov, M.R., et al., Astron. Lett., 30, 527.
- Ubertini, P., Lebrun. F., Di Cocco, G., et al. 2003, A&A, 411, L131
- Winkler, C., et al. 2004, ESA SP-552, 7

Table 3. 4th IBIS/ISGRI Catalog

Name <sup>a</sup>	RA	Dec	Error <sup>b</sup>	F20-40 <sup>c</sup>	F40-100 <sup>c</sup>	Type <sup>d</sup>	Vari <sup>e</sup>	Peak flux <sup>f</sup>	Signif <sup>g</sup>	Exposure <sup>h</sup>	MapCode <sup>i</sup>	
IGR J00040+7020	0.960	70.305	3.2	0.7±0.1	1.0±0.2	AGN,Sy2	Y	1.7±1.1	8.4	2013.7	B5	
<b>IGR J00158+5605</b>	3.961	56.032	4.9	0.5±0.1	< 0.3	AGN?	Y	1.7±1.1	5.1	3030.8	B1	
IGR J00234+6141	5.738	61.677	2.9	0.7±0.1	< 0.3	CV,IP	YY	21.3±0.9	9.2	3767.5	B4	
IGR J00245+6251	6.115	62.835	1.1	< 0.2	< 0.3	GRB	YY	28.6	3797.7	burst		
4U 0022+63	6.313	64.133	2.5	0.7±0.1	0.6±0.1	SNR	YY	10.5	3729.3	burst		
IGR J00256+6821	6.329	68.357	2.6	0.7±0.1	1.0±0.2	AGN,Sy2	Y	9.6	3174.2	B3		
V709 Cas	7.198	59.284	0.6	4.5±0.1	2.7±0.1	CV,IP	YY	56.9	3562.7	B5		
IGR J00291+5934	7.255	59.564	0.4	2.4±0.1	2.8±0.1	LMXB,XP,T	Y	29.8±0.3	113.3	3580.2	burst	
IGR J00333+6122	8.326	61.458	2.6	0.7±0.1	0.9±0.1	AGN,Sy1.5	Y	9.8	3700.7	B3		
1ES 00333+595	8.964	59.830	1.6	1.3±0.1	0.9±0.1	AGN,BL Lac	Y	18.2	3562.7	B4		
IGR J00370+6122	9.201	61.363	2.8	0.5±0.1	0.6±0.1	HMXB,XP,Sy?	Y	6.5±0.8	9.7	3641.2	burst	
<b>IGR J00451+3842</b>	11.276	38.711	4.8	2.1±0.5	< 1.9	?	Y	2.9±0.7	5.0	86.9	R346B4	
<b>IGR J00465-4005</b>	11.615	-40.087	4.8	1.1±0.4	2.9±0.7	AGN?	Y	4.9	134.6	burst		
MKN 348	12.178	31.952	2.0	5.5±0.5	6.8±0.9	AGN,Sy2	Y	14.1	105.0	B5		
RX J0053.8-7226	13.522	-72.445	3.2	2.7±0.4	1.8±0.7	HMXB,XP,Be,T	Y	8.2	140.4	burst		
<b>IGR J00556+7708</b>	13.895	77.134	4.9	< 0.5	< 0.9	AGN?	Y	5.2	536.2	S047B4		
gam Cas	14.166	60.712	0.7	4.3±0.1	1.2±0.1	HMXB,Be	Y	54.4	3295.8	B4		
IGR J01085-4550	17.115	-45.848	5.1	1.1±0.5	3.8±0.9	?	Y	4.8	102.7	B3		
<b>IGR J01170-1012</b>	19.240	-10.204	5.1	1.6±0.5	2.6±0.8	?	Y	5.8±2.0	4.8	126.5	B3	
SMC X-1	19.285	-73.447	0.4	36.3±0.4	7.2±0.7	HMXB,XP	YY	101.3	147.9	B4		
1A 0114+650	19.500	65.289	0.4	10.0±0.1	5.8±0.2	HMXB,XP	YY	111.5	2792.3	burst		
4U 0115+634	19.618	63.743	0.2	17.9±0.1	5.3±0.2	HMXB,XP,T	YY	332.7±0.4	843.7	2793.5	burst	
IGR J01191+0743	19.771	7.712	4.5	1.9±0.8	4.6±1.3	?	Y	5.3	76.7	B2		
<b>RX J0119.5-7301</b>	20.077	-73.059	5.0	1.3±0.4	< 1.3	cluster?	Y	5.0	141.4	B5		
NGC 526	20.978	-35.057	3.9	3.2±0.6	3.1±1.1	AGN,Sy1.5	Y	6.3	85.2	B5		
IGR J01295+5011	22.364	50.183	4.5	< 0.5	< 0.8	?	Y	7.0±3.3	5.5	771.5	R148B1	
IGR J01363+6610	24.059	66.192	3.7	< 0.2	< 0.4	HMXB,Be,T	YY	4.9±1.4	6.9	2277.1	R185B5	
<b>RX J0137.7+5814</b>	24.345	58.251	5.0	0.4±0.1	< 0.4	AGN,BL Lac	Y	1.6±0.3	5.1	1905.9	burst	
<b>ESO 297-18</b>	24.666	-40.015	4.4	2.8±0.6	4.2±1.1	AGN,Sy2	Y	5.9	101.7	S373B3		
4U 0142+614	26.594	61.751	1.2	1.6±0.1	4.3±0.2	AXP	Y	25.3	1965.9	B3		
RX J0146.9+6121	26.758	61.351	2.1	1.2±0.1	0.6±0.2	HMXB,XP,Be,T	Y	2.7±0.2	13.1	1925.5	burst	
IGR J01528-0326	28.214	-3.465	3.2	1.2±0.2	1.8±0.3	AGN,Sy2	Y	8.0	770.2	B3		
<b>IGR J01545+6437</b>	28.605	64.620	4.1	0.6±0.1	< 0.4	AGN?	Y	6.0	1851.9	B4		
<b>IGR J01583+6713</b>	29.523	67.213	2.0	0.5±0.1	< 0.5	HMXB,XP?,Be,T	Y	13.1±0.9	13.9	1724.8	burst	
NGC 788	30.280	-6.819	1.3	3.2±0.2	3.8±0.3	AGN,Sy2	Y	22.0	853.7	B5		
Mrk 1018	31.534	-0.284	4.0	1.0±0.2	1.0±0.3	AGN,Sy1.5	Y	6.6	857.3	B5		
<b>IGR J02086-1742</b>	32.131	-17.718	4.5	0.9±0.3	2.2±0.6	AGN?	Y	5.3	318.0	B3		

Table 3—Continued

Name <sup>a</sup>	RA	Dec	Error <sup>b</sup>	F20-40 <sup>c</sup>	F40-100 <sup>c</sup>	Type <sup>d</sup>	Vari <sup>e</sup>	Peak flux <sup>f</sup>	Sigfig <sup>g</sup>	Exposure <sup>h</sup>	MapCode <sup>i</sup>
IGR J02097+5222	32.436	52.425	2.8	1.6±0.2	1.7±0.4	AGN,Sy1			9.7	666.7	B5
<b>IGR J02115-4407</b>	32.866	-44.132	5.0	2.0±0.7	<2.4	?			4.6	67.5	B5
SWIFT J0216.3+5128	34.131	51.421	4.5	0.9±0.2	1.0±0.4	AGN,Sy2?			5.5	558.6	B5
<b>SWIFT J0218.0+7348</b>	34.398	73.833	3.8	1.2±0.2	1.9±0.4	AGN,BL Lac,HPQ			6.9	702.7	B3
<b>IGR J02343+3229</b>	38.564	32.518	5.0	2.4±0.6	3.1±1.1	AGN,Sy2	Y	5.3±1.5	4.6	85.0	R220B3
NGC 985	38.664	-8.806	3.8	0.9±0.2	1.8±0.3	AGN,Sy1			7.2	619.3	B3
<b>IGR J02378+1829</b>	39.457	18.490	5.1	2.6±0.6	<2.1	?			4.5	93.0	B5
LS I+61 303	40.119	61.240	2.5	1.4±0.2	2.1±0.3	HMXB,?,M			10.9	1023.0	B3
NGC 1052	40.252	-8.238	4.4	1.1±0.2	0.9±0.4	AGN,Sy2			5.9	613.6	B5
RBS 345	40.588	5.498	4.9	0.8±0.2	1.5±0.4	AGN,Sy1			5.1	522.4	B5
NGC 1068	40.689	0.005	3.0	1.5±0.2	1.3±0.3	AGN,Sy2			8.5	693.1	B3
<b>IGR J02447+7046</b>	41.178	70.775	4.6	<0.4	<0.8	AGN?	YY	26.0±6.7	5.4	773.6	R132B5
QSO B0241+62	41.231	62.466	1.6	2.6±0.2	3.4±0.3	AGN,Sy1			18.8	981.1	B5
IGR J02504+5443	42.635	54.709	3.5	1.1±0.2	1.1±0.4	AGN,Sy2			7.0	722.9	burst
NGC 1142	43.797	-0.175	1.6	3.6±0.2	3.6±0.4	AGN,Sy2			17.0	465.1	B5
<b>XY Ari</b>	44.017	19.440	4.3	1.9±0.5	2.0±0.9	CV,IP	Y	3.4±0.7	5.8	119.0	B5
NGC 1194	45.942	-1.147	5.1	0.9±0.3	2.0±0.5	AGN,Sy2			5.1	330.6	B3
<b>IGR J03103+5706</b>	47.570	57.102	4.9	<0.5	<0.8	AGN?			5.1	642.5	R146B4
B3 B0309+411B	48.244	41.370	4.6	1.8±0.3	<1.2	AGN,Sy1	Y	2.1±0.4	5.5	224.9	R220B1
<b>SWIFT J0318.7+6828</b>	49.760	68.430	4.8	1.2±0.3	<0.9	AGN,Sy1.9	Y	2.0±0.5	4.7	570.4	B1
<b>IGR J03199+7402</b>	49.964	74.043	5.5	1.6±0.4	1.6±0.7	?			4.8	302.9	B3
NGC 1275	49.967	41.532	2.4	2.8±0.3	1.8±0.6	AGN,Sy2			11.1	221.7	B4
1H 0323+342	51.144	34.213	4.0	2.0±0.5	2.6±0.8	AGN,Sy1			6.8	127.9	B5
GK Per	52.801	43.905	4.3	1.5±0.3	<1.1	CV,IP			5.2	277.9	burst
<b>NGC 1365</b>	53.400	-36.153	4.4	2.8±0.5	2.1±0.9	AGN,Sy1.8			5.7	115.9	B5
<b>IGR J03344+1506</b>	53.609	15.115	5.4	<0.9	2.1±0.8	AGN?			4.6	163.8	S463B3
EXO 0331+530	53.744	53.172	0.2	190.8±0.3	29.6±0.5	HMXB,XP,Be,T	Y	376.1±0.4	1521.8	424.1	burst
<b>ESO548-G01</b>	55.478	-21.258	3.9	1.9±0.5	3.2±0.9	AGN,Sy1			6.0	105.4	B3
<b>IGR J03502-2605</b>	57.548	-26.090	4.8	1.3±0.5	1.9±0.9	?			5.2	113.8	R458B5
IGR J03532-6829	58.261	-68.493	4.1	1.3±0.2	<0.8	AGN,BL Lac			6.4	478.7	B4
X Per	58.843	31.046	0.6	24.9±0.5	30.2±0.9	HMXB,XP,Be	Y		56.6	135.5	B5
<b>IGR J03564+6242</b>	59.099	62.714	4.6	0.9±0.3	1.8±0.6	?			5.1	292.6	burst
<b>3C 098</b>	59.686	10.420	4.1	1.5±0.3	3.0±0.6	AGN,Sy2			6.6	248.6	B3
<b>IGR J04069+5042</b>	61.730	50.702	4.2	1.6±0.3	<1.0	?			5.9	321.8	burst
<b>4C03.8</b>	61.856	3.702	3.6	1.7±0.3	2.3±0.6	AGN,NLRG			7.0	248.7	burst
3C 111	64.575	38.022	2.4	5.4±0.6	6.7±1.0	AGN,Sy1/BLRG			11.0	97.1	B5
<b>LEDA 15023</b>	65.951	4.145	3.8	1.1±0.3	1.1±0.5	AGN,Sy2			6.3	325.1	B5

Table 3—Continued

Name <sup>a</sup>	RA	Dec	Error <sup>b</sup>	F20-40 <sup>c</sup>	F40-100 <sup>c</sup>	Type <sup>d</sup>	Vari <sup>e</sup>	Peak flux <sup>f</sup>	Signif <sup>g</sup>	Exposure <sup>h</sup>	MapCode <sup>i</sup>	
<b>3C120</b>	68.294	5.348	1.5	4.2±0.2	5.1±0.5	AGN,Sy1/BLRG	Y	3.3±0.6	5.7	356.3	B5	
IGR J04343+5646	68.578	56.775	4.7	1.9±0.4	<1.3	?	Y	2.2±0.6	5.7	194.8	burst	
IGR J04412+5921	70.288	59.351	4.7	1.3±0.5	1.6±0.8	?	Y	2.2±0.6	5.7	163.0	burst	
<b>UGC 3142</b>	70.894	28.987	4.1	3.7±0.5	2.2±0.7	AGN,Sy1	?	7.5	204.2	B1		
IGR J04442+0450	71.043	4.849	4.6	0.6±0.3	<0.9	?	Y	4.7±0.9	5.4	361.0	S478B1	
IGR J04451-0445	71.273	-4.765	4.1	1.3±0.4	2.0±0.7	?	Y	2.1±0.5	6.7	172.3	burst	
LEDA 168563	73.031	49.530	3.2	3.1±0.5	3.4±0.8	AGN,Sy1	?	8.6	141.1	B5		
<b>SWIFT J0453.4+0404</b>	73.379	4.034	4.2	1.4±0.3	1.2±0.5	AGN,Sy2	?	6.6	347.9	B5		
ESO 033-G02	73.925	-75.551	2.6	1.7±0.2	1.2±0.3	AGN,Sy2	?	10.0	606.6	B4		
<b>4U 0504-84</b>	74.352	-84.268	5.0	0.6±0.3	1.6±0.5	?	Y	2.8±0.9	4.7	311.8	R154B3	
IGR J05007-7047	75.261	-70.779	3.5	<0.4	<0.6	HMXB,Be,T	YY	1.5±0.5	7.4	670.9	R027B4	
<b>SWIFT J0505.7-2348</b>	76.412	-23.839	3.0	2.9±0.4	3.5±0.7	AGN,Sy2,HII	?	8.2	191.8	B5		
4U 0517+17	77.694	16.494	2.0	3.8±0.3	4.2±0.4	AGN,Sy1.5	?	15.5	516.5	B1		
<b>4U 0513-40</b>	78.523	-40.061	3.3	2.8±0.4	<1.4	LMXB,B,G	?	7.3	181.2	B1		
<b>Ark 120</b>	79.047	-0.145	2.3	3.3±0.4	4.3±0.7	AGN,Sy1	?	11.2	235.9	B5		
<b>SWIFT J0519.5-3140</b>	79.906	-32.651	3.0	2.5±0.3	2.6±0.6	AGN,Sy2	?	8.9	272.5	B5		
<b>PICTOR A</b>	79.937	-45.784	5.2	2.2±0.5	<1.8	AGN,Sy1	?	4.8	117.1	B1		
IGR J05253+6447	81.317	64.792	4.4	<0.8	1.4±0.7	?	Y	3.1±0.8	5.4	244.5	S163B5	
IGR J05255-0711	81.374	-7.191	5.1	2.7±0.7	<2.6	?	Y	4.8	71.9	S478B5		
<b>3A 0527-329</b>	82.350	-32.811	2.2	3.5±0.3	<1.1	CW,IP	?	11.7	284.9	B4		
LMC X-4	83.206	-66.368	0.3	23.1±0.2	7.7±0.3	HMXB,XP	Y	49.3±0.3	185.0	654.9	burst	
<b>IGR J05346-5759</b>	83.617	-58.024	4.3	1.7±0.3	<1.0	CW,Nova like	?	5.8	363.6	B1		
Crab	83.629	22.017	0.2	999.9±0.2	1000.0±0.3	PVN,PSR	?	5625.3	818.8	B4		
1A 0535+262	84.729	26.321	0.2	6.5±0.3	4.0±0.4	HMXB,XP,Be,T	Y	178.7±1.8	667.1	588.0	S347B4	
LMC X-1	84.958	-69.754	1.1	2.3±0.2	1.5±0.3	HMXB,BH	Y	3.9±0.2	26.7	679.4	B4	
PSR B0540-69.3	85.043	-69.328	2.3	1.8±0.2	1.5±0.3	PVN,PSR	?	12.2	694.3	B5		
BY Cam	85.675	60.851	4.3	2.6±0.5	2.5±0.8	CW,P	?	6.3	162.6	B5		
<b>NGC 2110</b>	88.075	-7.445	2.3	8.6±1.0	12.1±1.7	AGN,Sy2	?	11.2	45.2	B5		
IGR J05535+0257	88.374	2.957	4.1	1.8±0.5	1.9±0.9	?	Y	5.5	111.9	S478B5		
MCG+08-11-011	88.739	46.453	3.5	5.2±0.8	4.8±1.3	AGN,Sy1.5	?	26.7	45.3	burst		
<b>4U 0557-385</b>	89.466	-38.334	4.5	1.9±0.4	<1.4	AGN,Sy1.5	Y	7.9	213.7	S490B4		
IGR J05583-1257	89.571	-12.962	4.8	2.5±0.9	4.1±1.5	AGN?	?	4.8	64.8	B2		
<b>IRAS 05589+2828</b>	90.523	28.429	3.5	2.2±0.3	2.5±0.5	AGN,Sy1	?	8.1	419.8	B4		
SWIFT J0601.9-8636	91.688	-86.596	3.5	1.3±0.3	1.7±0.6	AGN,Sy2	?	7.1	255.4	R099B5		
<b>IGR J06073-0024</b>	91.830	-0.415	4.8	1.6±0.6	<2.2	?	YY	7.9±1.7	5.1	79.0	R051B1	
Mrk 3	93.884	71.045	1.2	4.5±0.2	6.5±0.4	AGN,Sy2	?	25.7	546.0	B3		
4U 0614+091	94.280	9.135	0.8	21.2±0.6	15.6±0.8	LMXB,B,A	?	43.0	147.9	B5		

Table 3—Continued

Name <sup>a</sup>	RA	Dec	Error <sup>b</sup>	F20-40 <sup>c</sup>	F40-100 <sup>c</sup>	Type <sup>d</sup>	Vari <sup>e</sup>	Peak flux <sup>f</sup>	Signif <sup>g</sup>	Exposure <sup>h</sup>	MapCode <sup>i</sup>	
IGR J06239-6052	95.952	-60.943	4.6	1.3±0.3	< 0.9	AGN,Sy2?		5.8	348.4	B1		
IGR J06253+7334	96.375	73.563	4.6	1.0±0.2	< 0.8	CV,IP		5.4	548.2	B4		
<b>IGR J06293-1359</b>	97.327	-13.998	4.2	2.2±0.4	< 1.5	?		5.4	218.3	B1		
<b>SWIFT J0640-4-2554</b>	100.045	-25.830	5.1	2.2±0.6	2.3±1.0	AGN,Sy1.2		4.6	128.3	B5		
Mirk 6	103.044	74.421	2.0	2.1±0.2	2.9±0.4	AGN,Sy1.5		13.2	579.3	B5		
<b>IGR J06523+5334</b>	103.069	53.574	5.1	2.9±0.8	< 2.8	?	Y	3.2±0.9	4.9	71.1	B4	
<b>IGR J06552-1146</b>	103.792	-11.770	4.3	1.1±0.3	< 1.0	?	Y	2.6±1.0	5.8	399.9	B4	
<b>3A 0656-072</b>	104.576	-7.209	0.7	7.7±0.3	2.3±0.5	HMXB,XP,Be,T	Y	20.6±0.5	46.6	405.8	burst	
<b>IGR J07145+0056</b>	108.623	0.941	5.1	0.9±0.4	< 1.4	?	Y	4.6±1.0	4.8	221.7	S04TB4	
<b>IGR J07193-1233</b>	109.830	-12.556	4.9	< 0.5	< 0.9	? <sub>T</sub>		5.0	452.3	R420B3		
<b>IGR J07199-2521</b>	109.965	-25.365	4.2	< 0.8	< 1.3	? <sub>T</sub>	Y	5.5±1.5	6.2	227.1	R618B4	
<b>IGR J07225-3810</b>	110.621	-38.168	5.3	1.3±0.4	< 1.1	?	Y	2.3±0.5	4.9	272.8	burst	
<b>LEDA 96373</b>	111.614	-35.892	5.4	1.1±0.4	1.5±0.6	AGN,Sy2		4.7	232.1	B5		
<b>SWIFT J0732.5-1331</b>	113.159	-13.531	4.1	1.4±0.3	1.6±0.5	CV,IP		6.2	409.0	B3		
<b>IGR J07361-4537</b>	114.034	-45.618	4.5	< 0.4	< 0.5	? <sub>T</sub>	YY	11.8±2.2	5.4	1094.4	burst	
EXO 0748-676	117.135	-67.751	0.5	21.2±0.3	19.0±0.5	LMXB,B,D,T		76.5	315.1	B5		
<b>IGR J07506-1547</b>	117.675	-15.793	5.2	< 0.7	2.0±0.6	?	Y	1.7±0.7	5.1	281.4	burst	
IGR J07565-4139	119.086	-41.633	3.4	0.9±0.1	0.8±0.2	AGN,Sy2	Y	1.4±0.2	7.6	1582.2	burst	
IGR J07597-3842	119.927	-38.718	1.7	2.4±0.2	1.8±0.2	AGN,Sy1.2		16.5	1346.7	B5		
<b>1RXS J080114.6-462324</b>	120.284	-46.379	3.6	0.3±0.1	0.4±0.2	?	Y	5.5±0.9	7.4	2032.3	burst	
ESO 209-12	120.476	-49.762	2.3	1.1±0.1	1.5±0.2	AGN,Sy1.5		11.9	1931.5	B3		
PG0804+761	122.851	76.021	4.9	0.9±0.2	< 0.8	AGN,Sy1		4.6	523.9	B5		
<b>IGR J08190-3835</b>	124.759	-38.583	3.5	0.8±0.1	0.8±0.2	AGN?		7.4	2083.2	B3		
IGR J08262+4051	126.556	40.855	4.8	1.3±0.5	< 1.7	AGN?	Y	3.1±0.9	5.1	103.8	R314B4	
<b>IGR J08262-3736</b>	126.560	-37.603	4.3	0.4±0.1	0.7±0.2	?	Y	0.7±0.2	5.4	2126.9	burst	
Vela Pulsar	128.831	-45.179	0.5	6.8±0.1	7.4±0.1	PWN,PSR		89.1	2993.1	B5		
4U 0836-429	129.346	-42.895	0.2	16.8±0.1	14.8±0.1	LMXB,B,T	Y	73.9±0.2	435.5	3099.8	burst	
FRL 1146	129.633	-35.998	2.3	1.4±0.1	1.1±0.2	AGN,Sy1.5		11.5	1934.1	B5		
<b>IGR J08390-4833</b>	129.692	-48.532	3.8	0.4±0.1	< 0.3	CV,IP	Y	0.8±0.1	7.1	3072.1	burst	
IGR J08408-4503	130.159	-45.067	3.3	0.3±0.1	< 0.3	HMXB,SFXT	Y	6.3±0.8	9.0	3227.4	burst	
QSO B0836+710	130.343	70.901	2.0	2.4±0.2	4.2±0.4	AGN,Bazar		14.4	511.5	B3		
<b>IGR J08517-1827</b>	132.931	-18.452	4.6	2.2±0.6	< 2.0	?	Y	6.0±1.1	5.4	114.9	R313B1	
<b>IGR J08558+0814</b>	133.957	8.248	5.0	2.0±0.6	< 2.1	AGN,Sy1	Y	4.0±1.1	4.5	89.4	B4	
Vela X-1	135.524	-40.555	0.2	216.9±0.1	54.3±0.2	HMXB,XP			2259.9	2987.3	B1	
IGR J09025-6814	135.582	-68.225	5.0	1.1±0.3	1.2±0.5	AGN,XBONG	Y	2.0±0.4	4.8	413.0	S192B3	
IGR J09026-4812	135.658	-48.222	1.7	1.2±0.1	1.6±0.1	AGN,Sy1		16.8	3123.4	B3		
<b>1RXS J090320.0+533022</b>	135.853	53.498	5.3	2.2±0.8	< 2.8	AGN?		4.7	46.8	B4		

Table 3—Continued

Name <sup>a</sup>	RA	Dec	Error <sup>b</sup>	F20-40 <sup>c</sup>	F40-100 <sup>c</sup>	Type <sup>d</sup>	Vari <sup>e</sup>	Peak flux <sup>f</sup>	Signif <sup>g</sup>	Exposure <sup>h</sup>	MapCode <sup>i</sup>
IGR J09103-3741	137.577	-37.682	5.4	< 0.3	< 0.4	? <sub>T</sub>			4.5	1770.0	R317B1
SWIFT J0917.2-6221	139.069	-62.338	2.7	1.4±0.2	0.9±0.3	AGN,Sy1.2			9.8	1332.5	B5
<b>IGR J09189-4418</b>	139.731	-44.312	4.5	0.3±0.1	0.5±0.2	?			5.4	2949.8	B2
EXMS B0918-549E	140.052	-55.126	1.0	2.8±0.1	2.1±0.2	? <sub>T</sub>			32.0	2263.7	B5
4U0919-54	140.095	-55.197	0.9	3.7±0.1	2.8±0.2	LMXB			34.0	2259.8	B5
<b>MCG-01-24-012</b>	140.174	-8.075	4.2	1.5±0.4	3.1±0.7	AGN,Sy2			6.0	170.7	B3
<b>Mrk 110</b>	141.249	52.309	4.4	3.2±0.8	2.8±1.4	AGN,Sy1			5.6	44.8	B5
IGR J09253+6929	141.345	69.520	4.9	1.2±0.3	< 1.1	AGN,Sy1.5			5.4	289.2	B5
<b>IGR J09446-2636</b>	146.148	-26.605	5.4	1.1±0.5	< 1.6	AGN,Sy1.5			4.5	157.8	burst
<b>IGR J09453-2600</b>	146.333	-26.003	4.5	1.5±0.5	< 1.5	? <sub>T</sub>			5.5	166.3	burst
<b>NGC 2992</b>	146.425	-14.343	1.9	3.5±0.3	4.1±0.5	AGN,Sy2			14.8	272.0	B5
MCG-05-23-016	146.912	-30.952	1.4	8.4±0.4	8.6±0.7	AGN,Sy2			20.7	183.5	B3
<b>IGR J09480-5641</b>	147.010	-56.697	4.9	< 0.2	< 0.4	? <sub>T</sub>			5.1	1984.9	R229B5
<b>IGR J09481+8237</b>	147.034	82.629	4.5	2.0±0.5	< 1.5	?			4.8	207.4	B1
IGR J09523-6231	148.058	-62.522	3.2	0.9±0.1	0.8±0.2	AGN,Sy1.9			8.4	1607.6	B5
<b>NGC 3081</b>	149.872	-22.809	2.4	3.2±0.4	3.7±0.6	AGN,Sy2			10.8	225.6	B5
SWIFT J1009.3-4250	152.419	-42.804	2.8	1.6±0.2	1.7±0.3	AGN,Sy2			9.7	1020.0	B5
GRO J1008-57	152.435	-58.295	0.5	4.0±0.1	2.0±0.2	HMXB,XP,Be,T			83.8	1998.5	burst
IGR J10101-5654	152.506	-56.922	2.3	1.0±0.1	0.6±0.2	HMXB,Be			12.1	1973.0	burst
IGR J10109-5746	152.732	-57.800	2.4	1.1±0.1	< 0.4	CV,Symb			11.2	2045.3	B4
IGR J10147-6354	153.669	-63.898	4.9	< 0.3	0.9±0.2	AGN,Sy1.2			5.0	1810.5	burst
<b>IGR J10163-5028</b>	154.071	-50.481	4.9	< 0.3	< 0.4	? <sub>T</sub>			5.1	1527.3	R399B5
IGR J10200-1436	155.007	-14.611	4.9	1.6±0.4	< 1.4	?			4.7	181.6	burst
<b>NGC 3227</b>	155.871	19.858	1.9	6.8±0.5	6.5±0.9	AGN,Sy1.5			15.0	91.6	B5
<b>IGR J10252-6829</b>	156.221	-68.516	5.0	< 0.3	0.6±0.3	? <sub>T</sub>			5.0	1103.4	burst
NGC 3281	157.950	-34.870	3.3	2.4±0.4	3.5±0.7	AGN,Sy2			7.4	182.3	B5
<b>IGR J10344+1401</b>	158.604	14.017	4.3	2.4±0.9	< 3.2	?			5.9	37.4	S262B1
4U 1036-56	159.425	-56.798	1.3	1.1±0.1	< 0.4	HMXB,Be,T			22.3	2079.8	burst
SWIFT J1038.8-4942	159.665	-49.801	3.5	0.9±0.1	1.4±0.2	AGN,Sy1.5			8.0	1243.9	B3
IGR J10404-4625	160.108	-46.413	2.7	1.7±0.2	2.2±0.3	XB			9.6	781.1	B3
<b>IGR J10432-6300</b>	160.802	-63.013	4.4	< 0.2	< 0.4	? <sub>T</sub>			5.7	2100.3	R325B1
IGR J10432-4446	160.805	-44.779	4.6	< 0.5	1.2±0.4	?			5.4	547.0	S081B3
<b>IGR J10447-6027</b>	161.155	-60.423	4.1	0.6±0.1	0.7±0.2	?			5.8	2188.9	B5
Eta Carinae	161.206	-59.704	4.3	0.3±0.1	0.7±0.2	AGN			5.9	2208.1	burst
<b>MCG+04-26-006</b>	161.722	25.903	5.0	1.1±0.3	2.5±0.6	?			5.2	230.7	B3
<b>IGR J111014-6103</b>	165.341	-61.056	4.3	0.4±0.1	0.6±0.2	AGN, BL Lac			5.4	2287.7	B3
<b>Mrk 421</b>	166.119	38.207	0.3	25.6±0.2	19.4±0.4	AGN, BL Lac			151.1	607.9	S448B5

Table 3—Continued

Name <sup>a</sup>	RA	Dec	Error <sup>b</sup>	F20-40 <sup>c</sup>	F40-100 <sup>c</sup>	Type <sup>d</sup>	Vari <sup>e</sup>	Peak flux <sup>f</sup>	Signif <sup>g</sup>	Exposure <sup>h</sup>	MapCode <sup>i</sup>
IGR J1098-6457	167.389	-64.956	5.0	0.4±0.1	0.6±0.2	CV,Symb	Y	0.7±0.2	5.1	2129.5	burst
IGR J11187-5438	169.612	-54.653	4.1	0.6±0.1	0.7±0.2	XB?			6.1	2030.4	B5
Cen X-3	170.306	-60.627	0.2	54.6±0.1	5.9±0.2	HMXB,XP			650.7	2467.0	burst
IGR J11215-5952	170.440	-59.870	1.5	0.3±0.1	<0.3	HMXB,SFXT	YY	10.2±0.6	19.8	2405.1	R308B5
IGR J11305-6256	172.779	-62.946	0.9	3.3±0.1	1.5±0.2	HMXB,Be			35.1	2378.1	burst
<b>IGR J11321-5311</b>	173.007	-53.199	3.5	<0.3	<0.4	AXP?,T	YY	7.3±1.5	7.1	1847.8	burst
IGR J11366-6002	174.140	-60.047	4.2	0.6±0.1	0.6±0.2	AGN,Sy2,Liner			6.0	2431.5	B3
NGC 3783	174.746	-37.745	2.9	8.4±1.0	7.4±1.7	AGN,Sy1			9.0	42.1	B5
EXMS B1136-650	174.850	-65.386	1.8	0.4±0.1	<0.4	RSCVn	YY	24.2±1.6	15.6	2253.9	burst
IGR J11435-6109	175.976	-61.127	0.7	3.4±0.1	2.2±0.2	HMXB,XP?,Be	Y	13.0±0.3	53.4	2484.2	burst
<b>H1143-182</b>	176.416	-18.445	4.6	3.6±0.7	<2.3	AGN,Sy1			5.4	92.4	B1
<b>PKS 1143-696</b>	176.449	-69.894	4.1	0.8±0.2	0.8±0.2	AGN	Y	1.3±0.2	6.2	1453.3	burst
1E 1145.1-6141j	176.852	-61.966	0.3	21.1±0.1	12.2±0.2	HMXB,XP			206.5	2457.1	B5
2E 1145.5-6155j	176.968	-62.212	0.9	2.4±0.1	1.7±0.2	HMXB,XP	Y	22.3±0.7	37.1	2487.0	burst
<b>IGR J11486-0505</b>	177.160	-5.098	5.4	1.2±0.3	<0.9	?T	Y	7.5±1.5	4.9	470.1	R268B1
IGR J11502-5427	177.542	-54.463	4.6	<0.3	<0.4	?			5.4	1985.7	S155B1
<b>IGR J11544-7618</b>	178.592	-76.309	5.0	0.9±0.4	2.3±0.6	AGN?			4.7	339.7	B3
<b>IGR J11592+1437</b>	179.809	14.621	5.0	<0.7	<1.3	?T			4.9	271.7	S331B5
<b>IGR J11597-6324</b>	179.920	-63.408	4.5	<0.2	<0.4	?T			5.6	2318.8	R579B1
<b>SWIFT J1200.8+0650</b>	180.257	6.780	5.0	0.9±0.2	1.1±0.4	AGN,Sy2			5.0	600.5	B5
IGR J12026-5349	180.672	-53.841	1.5	2.3±0.1	2.1±0.2	AGN,Sy2			20.2	1804.9	B5
<b>NGC 4051</b>	180.802	44.508	2.5	2.5±0.2	1.8±0.4	AGN,Sy1.5			10.0	527.6	B1
<b>NGC 4074</b>	181.136	20.249	5.0	0.9±0.4	1.6±0.6	AGN,Sy2			5.1	258.5	B5
<b>IGR J12077-6547</b>	181.925	-65.789	4.4	<0.2	<0.4	?T			5.6	2296.8	burst
NGC 4138	182.359	43.719	3.7	1.6±0.2	1.5±0.4	AGN,Sy1.9			7.1	519.4	B5
NGC 4151	182.634	39.412	0.5	15.6±0.2	19.8±0.4	AGN,Sy1.5			85.4	490.5	B5
<b>IGR J12123-5802</b>	183.064	-58.049	4.4	0.5±0.1	<0.4	?			5.6	2234.5	B4
EXMS B1210-645	183.251	-64.871	3.0	0.9±0.1	0.6±0.2	HMXB,Be,T			8.8	2388.4	B5
IGR J12131+0700	183.280	7.018	4.3	0.8±0.2	1.2±0.3	AGN,Sy1.5-1.8			5.7	854.9	B3
<b>NGC4235</b>	184.296	7.159	5.1	0.5±0.2	<0.6	AGN,Sy1			4.5	914.7	B5
<b>Mrk 766</b>	184.603	29.823	3.7	1.4±0.2	0.8±0.3	AGN,Sy1			7.1	583.8	B1
4C 04.42	185.581	4.243	3.1	0.8±0.1	1.8±0.3	AGN,QSO			8.9	1136.3	burst
Mrk 50	185.806	2.670	3.5	1.1±0.1	<0.5	AGN,Sy1			8.5	1225.4	B1
NGC 4395	186.440	33.565	3.7	0.9±0.2	1.5±0.3	AGN,Sy1.8			7.2	620.0	B5
NGC 4388	186.448	12.657	0.5	12.6±0.2	16.0±0.4	AGN,Sy2			71.4	630.7	B5
GX 301-2	186.647	-62.774	0.2	155.1±0.1	18.1±0.2	HMXB,XP,T			1626.0	2504.7	B4
XSS J12270-4859	187.009	-48.894	2.5	1.6±0.2	1.6±0.3	CV,IP			10.5	955.6	B5

Table 3—Continued

Name <sup>a</sup>	RA	Dec	Error <sup>b</sup>	F20-40 <sup>c</sup>	F40-100 <sup>c</sup>	Type <sup>d</sup>	Vari <sup>e</sup>	Peak flux <sup>f</sup>	Signif <sup>g</sup>	Exposure <sup>h</sup>	MapCode <sup>i</sup>
<b>IGR J12288+0052</b>	187.199	0.870	5.3	0.6±0.1	<0.5	AGN?			4.7	1359.1	B5
3C 273	187.279	2.049	0.5	10.4±0.1	12.3±0.2	AGN,QSO			90.3	1334.5	B5
<b>IGR J12319-0749</b>	187.977	-7.816	4.7	0.6±0.1	<0.5	AGN?			4.8	1256.3	burst
V* RF Cru	188.724	-64.567	0.9	3.8±0.1	2.5±0.2	CV,Symb			37.3	2343.9	B5
NGC 4507	188.903	-39.912	0.9	8.4±0.3	10.6±0.5	AGN,Sy2			35.3	392.7	B5
ESO 506-G27	189.732	-27.303	2.8	4.4±0.6	5.3±0.9	AGN,Sy2			9.3	121.4	burst
LEDA 170194	189.786	-16.182	2.3	2.0±0.2	2.4±0.4	AGN,Sy2			11.5	572.6	B5
NGC 4593	189.909	-5.356	0.9	3.8±0.1	4.5±0.2	AGN,Sy1			35.5	1408.3	B5
IGR J12415-5750	190.331	-57.840	2.4	1.2±0.1	1.2±0.2	AGN,Sy1.5			11.0	2100.9	B5
1H 1249-637	190.663	-63.015	4.5	0.6±0.1	<0.4	HMXB,Be?			6.0	2284.1	B4
<b>IGR J12470-5407</b>	191.750	-54.129	5.3	<0.3	<0.4	?			4.7	1778.5	S338B1
<b>IGR J1248.2-5828</b>	191.943	-58.487	3.4	0.6±0.1	0.6±0.2	AGN	Y		6.8	2240.5	burst
<b>IGR J12489-6243</b>	192.223	-62.718	4.1	0.5±0.1	<0.4	?	Y		6.5	2277.5	burst
4U 1246-588	192.401	-59.093	0.8	3.8±0.1	3.2±0.2	HMXB,T			38.4	2246.4	B5
<b>NGC4748</b>	193.050	-13.430	5.5	0.8±0.2	0.7±0.3	AGN,NLSy1			5.2	841.4	B5
ESO 323-32	193.371	-41.620	4.3	0.9±0.2	1.2±0.4	AGN,Sy2			5.9	612.5	burst
3C 279	194.044	-5.770	2.5	1.1±0.1	1.4±0.2	AGN,QSO/Blazar			10.7	1248.5	burst
<b>IGR J12562+2554</b>	194.051	25.905	4.7	0.6±0.1	0.9±0.3	Cluster?			5.1	975.0	B5
1H 1254-690	194.410	-69.297	1.2	2.4±0.1	<0.5	LMXB,B,D			24.3	1749.2	B4
<b>IGR J12585-6045</b>	194.634	-60.765	4.9	0.3±0.1	<0.4	?,T	Y	2.7±1.1	5.0	2366.3	S511B4
Coma cluster	194.915	27.955	2.0	1.4±0.1	<0.5	Cluster			13.4	1053.4	B4
<b>GX 304-1</b>	195.340	-61.602	2.5	0.7±0.1	0.4±0.2	HMXB,XP	Y	2.9±0.3	10.7	2412.8	burst
IGR J13020-6359j	195.530	-63.949	1.6	2.0±0.1	1.1±0.2	HMXB,XP,Be			18.4	2342.9	B5
<b>PSR B1259-63<sup>j</sup></b>	195.658	-63.856	2.5	1.1±0.1	1.1±0.2	PSR			11.1	2362.1	burst
<b>Mrk 783</b>	195.753	16.362	4.6	0.8±0.2	1.7±0.4	AGN,Sy1			5.8	625.8	B3
<b>IGR J13038+5348</b>	195.924	53.773	4.8	1.0±0.3	2.1±0.5	AGN,Sy1.2			5.2	291.3	B3
NGC 4941	196.052	-5.570	4.6	0.7±0.1	0.6±0.3	AGN,Sy2			5.5	1079.0	B5
<b>IGR J13042-1020</b>	196.075	-10.344	4.1	1.0±0.2	0.7±0.3	AGN,Sy2			6.2	899.2	B5
<b>IGR J13045-5630</b>	196.133	-56.500	3.6	0.8±0.1	0.4±0.2	?			6.8	2099.5	B1
NGC 4945	196.362	-49.470	0.4	11.9±0.2	17.6±0.3	AGN,Sy2			96.6	1269.1	B3
ESO 323-77	196.619	-40.427	2.9	1.5±0.2	1.6±0.3	AGN,Sy1.2			9.0	649.2	B5
IGR J13091+1137	197.287	11.626	2.8	1.8±0.3	2.6±0.5	AGN,Sy2,XBONG			9.0	494.7	B3
<b>IGR J13107-5626</b>	197.669	-56.448	4.0	0.5±0.1	0.5±0.2	?			5.6	2105.2	B5
IGR J13109-5552	197.697	-55.868	2.3	1.1±0.1	1.7±0.2	AGN,Sy1			11.7	2028.9	B3
<b>IGR J13149+4422</b>	198.770	44.414	4.1	1.1±0.2	1.4±0.4	AGN,Sy2			6.2	577.0	B5
IGR J13186-6257	199.630	-62.944	3.3	0.7±0.1	0.5±0.2	?			7.7	2363.7	B5
<b>IGR J13187+0322</b>	199.665	3.372	4.9	<0.4	<0.8	AGN?,QSO?,T			5.0	641.7	R455B1

Table 3—Continued

Name <sup>a</sup>	RA	Dec	Error <sup>b</sup>	F20-40 <sup>c</sup>	F40-100 <sup>c</sup>	Type <sup>d</sup>	Vari <sup>e</sup>	Peak flux <sup>f</sup>	Signif <sup>g</sup>	Exposure <sup>h</sup>	MapCode <sup>i</sup>	
<b>MCG-03-34-063</b>	200.632	-16.726	4.8	1.1±0.3	1.6±0.6	AGN,Sy1.8	Y	6.8±2.0	5.0	352.0	B5	
<b>SAX J1324.3-6313</b>	201.161	-63.228	4.3	0.3±0.1	< 0.4	LMXB,B	Y	6.3	2361.5	R050B5	B5	
Cen A	201.363	-43.021	0.3	32.2±0.2	40.0±0.3	AGN,Sy2	YY	2.4±0.5	91.9	899.9	B5	
4U 1323-62	201.642	-62.139	0.5	8.7±0.1	6.5±0.2	LMXB,B,D	?	5.9	2378.2	burst		
<b>IGR J13290-6323</b>	202.261	-63.391	4.0	< 0.2	< 0.4	?	T	1.1±0.2	6.1	2333.5	burst	
<b>IGR J13292-6042</b>	202.302	-60.702	4.2	0.5±0.1	< 0.4	?	T	2.8±0.5	6.2	2382.2	burst	
<b>IGR J13307-6038</b>	202.671	-60.633	4.1	< 0.2	< 0.4	?	T	4.9	2377.1	R176B3		
<b>3C287.1</b>	203.184	2.017	5.2	1.5±0.3	< 1.1	AGN,Sy1	YY	4.9	381.0	B1		
<b>ESO 383-18</b>	203.382	-34.073	4.7	1.0±0.2	< 0.8	AGN,Sy2	YY	5.7	548.3	B4		
MCG-06-30-015	203.982	-34.300	1.8	3.1±0.2	1.9±0.4	AGN,Sy1.2	YY	15.2	571.6	B5		
NGC 5252	204.551	4.525	3.3	3.3±0.5	2.4±0.8	AGN,Sy1.9	YY	7.9	218.3	burst		
<b>IGR J13396-3306</b>	204.892	-33.101	5.0	0.8±0.2	< 0.8	?	?	4.9	523.7	B5		
<b>IGR J13402-6428</b>	205.050	-64.480	3.5	0.3±0.1	< 0.4	?	?	7.5	2317.0	burst		
<b>IGR J13408-6836</b>	205.191	-68.615	5.1	< 0.3	< 0.4	?	T	4.9	1874.6	burst		
<b>IGR J13415+3033</b>	205.336	30.380	3.8	1.2±0.2	1.0±0.3	AGN,Sy2	YY	6.5	682.4	B5		
<b>IGR J13439+0449</b>	205.974	4.817	5.1	2.1±0.6	2.1±1.0	?	?	4.5	137.9	burst		
Cen B <sub>j</sub>	206.704	-60.408	0.0	1.0±0.1	1.2±0.2	AGN,RG	YY	10.5	2332.1	B1		
4U 1344-60 <sup>j</sup>	206.882	-60.609	0.8	4.2±0.1	4.3±0.2	AGN,Sy1.5	YY	43.5	2323.7	B5		
<b>IGR J13490-6139</b>	207.257	-61.650	4.9	< 0.2	< 0.4	?	T	5.1	2358.2	R638B1		
IC 4329A	207.333	-30.313	0.6	11.8±0.2	12.7±0.4	AGN,Sy1.2	YY	55.6	442.5	B5		
<b>IGR J13499-4832</b>	207.468	-48.543	4.7	< 0.3	< 0.5	?	T	5.3	1486.5	burst		
<b>1AXG J135417-3746</b>	208.511	-37.767	4.4	1.0±0.2	0.7±0.3	AGN,Sy1.9	YY	10.5	2305.0	B3		
<b>IGR J13550-7218</b>	208.759	-72.299	4.2	0.6±0.2	1.1±0.3	?	?	5.8	1054.4	B1		
<b>IGR J13573-0845</b>	209.333	-8.764	5.4	2.5±0.7	< 2.4	?	?	4.7	70.7	B4		
IGR J14003-6326	210.217	-63.426	3.3	0.8±0.1	0.8±0.2	?	?	8.0	2222.9	B5		
<b>IGR J14043-6148</b>	211.070	-61.813	4.5	0.6±0.1	0.8±0.2	AGN?	YY	6.4	1675.7	R644B5		
<b>IGR J14080-3023</b>	212.009	-30.392	3.8	1.0±0.2	1.2±0.4	AGN,Sy1.5	YY	9.0	245.5	B5		
V834 Cen	212.219	-45.286	4.1	0.8±0.1	< 0.5	CV,P	YY	6.1	20.6	2318.6	B5	
<b>IGR J14102+0722</b>	212.549	7.377	4.5	4.7±1.7	< 5.7	?	?	5.2	629.7	H 1417-624		
NGC 5506	213.288	-3.206	2.9	11.3±1.5	6.7±2.5	AGN,Sy1.9	YY	126.4	2124.8	H 1419+480		
Circinus Galaxy	213.292	-65.343	0.4	13.1±0.1	10.9±0.2	AGN,Sy2	YY	8.2	1788.3			
IGR J14175-4641	214.265	-46.675	3.2	0.9±0.1	1.0±0.2	AGN,Sy2	YY	5.8	245.5			
<b>NGC 5548</b>	214.507	25.164	4.8	1.6±0.3	1.9±0.6	AGN,Sy1.5	YY	5.0	2318.6			
<b>IGR J14193-6048</b>	214.821	-60.801	4.3	0.5±0.1	< 0.4	?	?	5.6	2244.1			
ESO 511-G030	214.837	-26.640	3.0	1.9±0.2	2.1±0.4	AGN,Sy1	YY	401.4	401.4			
H 1417-624	215.255	-62.702	4.1	< 0.2	< 0.4	HMXB,XP,T	YY	6.1	2244.1			
H 1419+480	215.374	47.740	4.9	1.2±0.2	< 0.9	AGN,Sy1.5	YY	5.6	401.4			

Table 3—Continued

Name <sup>a</sup>	RA	Dec	Error <sup>b</sup>	F20-40 <sup>c</sup>	F40-100 <sup>c</sup>	Type <sup>d</sup>	Varie <sup>e</sup>	Peak flux <sup>f</sup>	Signif <sup>g</sup>	Exposure <sup>h</sup>	MapCode <sup>i</sup>
IGR J14227-2931	215.683	-29.519	5.0	0.5±0.2	< 0.6	?	Y	0.7±0.2	4.6	983.7	B4
IGR J14229-3347	215.728	-33.792	4.2	< 0.3	0.6±0.3	? , T	Y	2.7±0.7	6.0	1441.5	R533B3
IGR J14257-4249	216.427	-42.832	5.1	0.6±0.1	0.7±0.2	?			5.3	1911.5	B3
H 1426+428	217.136	42.652	4.4	1.0±0.2	1.1±0.5	AGN,BL Lac			5.6	377.9	B5
IGR J14297-5623	217.415	-56.396	4.4	< 0.2	< 0.4	? , T	YY	9.2±2.7	5.7	2338.3	R291B4
IGR J14298-6715	217.430	-67.255	3.3	0.9±0.1	0.9±0.2	LMXB			8.2	1847.5	B5
IGR J14300-2558	217.509	-25.982	4.5	0.8±0.2	< 0.8	?			4.8	701.5	burst
IGR J14301-4158	217.518	-41.979	4.9	0.6±0.1	0.5±0.2	?			5.4	1953.8	
IGR J14315-7046	217.878	-70.773	4.3	< 0.3	< 0.5	? , T	YY	3.4±0.8	5.8	1312.9	R091B3
NGC 5643	218.154	-44.180	3.8	0.7±0.1	0.6±0.2	AGN,Sy2			6.7	1961.0	B5
IGR J14331-6112	218.299	-61.248	3.5	0.8±0.1	< 0.4	HMXB,Be			7.3	2348.9	B5
IGR J14385+8553	219.616	85.883	4.9	< 0.7	< 1.2	?			5.0	229.3	B2
NGC 5728	220.597	-17.281	4.3	3.0±0.7	3.3±1.2	AGN,Sy2			5.6	100.2	B5
IGR J14471-6414	221.566	-64.287	4.1	0.6±0.1	0.7±0.2	AGN,Sy1.2			6.1	2011.3	B5
IGR J14466-3352	221.656	-33.869	4.4	0.4±0.1	1.0±0.2	?	Y	0.9±0.2	5.4	1772.7	B3
IGR J14471-6319	221.866	-63.306	3.3	0.8±0.1	0.8±0.2	AGN,Sy2			7.8	2145.2	burst
IGR J14488-5942	222.205	-59.701	4.3	0.5±0.1	< 0.4	? , T	Y	2.9±0.5	7.0	2415.3	R520B4
IGR J14488-4008	222.209	-40.142	4.4	0.5±0.1	< 0.4	AGN?			5.6	2140.3	burst
IGR J14492-5335	222.289	-53.596	2.4	1.0±0.1	1.3±0.2	AGN			11.6	2568.6	B5
IGR J14515-5542	222.888	-55.676	2.4	1.0±0.1	1.4±0.2	AGN,Sy2			11.4	2616.8	burst
IGR J14526+4925	223.162	49.426	5.4	0.8±0.3	1.2±0.6	?			4.6	270.0	S067B5
IGR J14536-5522	223.418	-55.369	1.9	1.3±0.1	0.5±0.2	CV,IP?	Y	1.9±0.1	14.9	2658.4	burst
IGR J14549-6459	223.713	-64.988	5.0	0.6±0.1	0.5±0.2	?			4.8	1962.5	B3
IGR J14552-5133	223.835	-51.589	3.1	0.8±0.1	0.9±0.2	AGN,NLSy1			8.8	2558.3	B5
IGR J14561-3738	224.034	-37.638	2.8	0.8±0.1	1.0±0.2	AGN,Sy2			9.4	2120.4	B5
IC 4518A	224.413	-43.133	1.8	1.5±0.1	1.0±0.2	AGN,Sy2			15.7	2279.7	B5
MKN 841	225.988	10.382	5.1	2.0±0.6	< 2.0	AGN,Sy1	Y	2.1±0.6	4.7	83.7	B5
IGR J15077+0906	226.932	9.109	4.6	1.8±0.6	2.5±1.0	?			5.2	83.2	B5
IGR J15094-6649	227.380	-66.822	2.4	1.5±0.1	0.8±0.2	CV,IP			12.0	1633.9	B5
IGR J15107-5414	227.670	-54.241	4.5	< 0.2	< 0.4	? , T	YY	8.9±1.7	5.7	2956.6	burst
IRAS 15091-2107	227.975	-21.356	4.9	1.6±0.4	< 1.3	AGN,NLSy1			4.5	257.7	B1
PSR B1509-58	228.486	-59.145	0.5	8.6±0.1	10.9±0.2	PSR			93.4	2555.3	B5
IGR J15161-3827	229.029	-38.476	5.7	< 0.2	0.5±0.2	AGN,Sy2	Y	0.3±0.2	4.5	2331.7	burst
Cir X-1	230.171	-57.170	0.4	7.3±0.1	0.4±0.2	LMXB,B,A,T			111.8	2774.7	burst
IGR J15293-5609	232.316	-56.163	5.4	< 0.2	< 0.3	?	Y	0.3±0.2	4.5	3017.0	S402B3
IGR J15311-3737	232.767	-37.625	4.5	0.3±0.1	0.7±0.2	?			5.1	2217.6	B2
IGR J15359-5750	234.000	-57.817	2.2	1.1±0.1	1.3±0.2	AGN?			12.5	2839.6	B5

Table 3—Continued

Name <sup>a</sup>	RA	Dec	Error <sup>b</sup>	F20-40 <sup>c</sup>	F40-100 <sup>c</sup>	Type <sup>d</sup>	Vari <sup>e</sup>	Peak flux <sup>f</sup>	Signif <sup>g</sup>	Exposure <sup>h</sup>	MapCode <sup>i</sup>
<b>IGR J15368-5102</b>	234.197	-51.045	4.9	0.5±0.1	< 0.3	?	Y	0.8±0.2	5.1	3329.7	burst
<b>IGR J15391-5307</b>	234.769	-53.116	4.5	0.5±0.1	0.3±0.2	?	YY	8.4±2.4	5.3	3358.5	burst
<b>IGR J15409-4057</b>	235.228	-40.960	4.8	< 0.2	< 0.4	?;T			5.2	2562.2	R166B4
<b>IGR J15415-5029</b>	235.369	-50.491	3.8	0.6±0.1	0.7±0.2	AGN?			7.0	3491.0	B3
4U 1538-522	235.596	-52.388	0.3	20.8±0.1	3.4±0.2	HMXB,XP			214.3	3503.2	B4
XTE J1543-568	236.023	-56.774	1.4	0.8±0.1	0.8±0.2	HMXB,XP,Be,T	Y	14.9±0.7	22.1	3020.4	burst
4U 1543-624	236.966	-62.575	1.1	3.0±0.1	1.1±0.2	LMXB,NS?			27.9	1888.3	B4
IGR J15479-4529	237.056	-45.481	0.7	5.1±0.1	3.1±0.2	CV,IP			52.0	3141.5	B5
NGC 5995	237.124	-13.765	2.4	2.1±0.3	2.0±0.5	AGN,Sy2			10.8	349.3	B3
XTE J1550-564	237.746	-56.479	0.2	20.5±0.1	33.1±0.2	LMXB,BH,T,M	Y	239.6±0.3	936.0	3099.8	burst
IGR J15529-5029	238.219	-50.500	3.5	0.7±0.1	< 0.3	CV?			7.4	3521.2	B1
IGR J15539-6142	238.357	-61.686	3.8	0.6±0.1	1.2±0.2	AGN,Sy2			6.7	2003.3	burst
<b>IGR J15549-3740</b>	238.721	-37.670	3.5	0.9±0.1	1.1±0.2	AGN?			7.4	1850.3	B3
1H 1556-605	240.297	-60.734	2.4	0.9±0.1	< 0.4	LMXB			11.7	2144.2	B4
<b>IGR J16016-3431</b>	240.408	-34.528	4.9	0.7±0.2	< 0.5	?	Y	1.3±0.3	5.2	1401.3	burst
IGR J16024-6107	240.553	-61.163	4.2	0.6±0.1	0.5±0.2	AGN,Sy2	Y	1.4±0.2	6.0	2022.0	burst
IGR J16056-6110	241.427	-61.219	3.9	0.6±0.1	0.9±0.2	AGN,Sy1.5			5.8	2000.7	B3
<b>IGR J16095-3710</b>	242.371	-37.179	4.6	0.5±0.2	1.0±0.2	?	Y	1.0±0.3	5.6	1643.5	burst
IGR J16119-6036	243.009	-60.634	2.1	1.6±0.1	1.4±0.2	AGN,Sy1			13.7	2057.4	B5
4U 1608-522	243.181	-52.426	0.3	15.2±0.1	9.9±0.1	LMXB,B,A,T	Y	41.0±0.2	250.7	3357.4	burst
IGR J16167-4957	244.154	-49.974	1.3	2.0±0.1	0.7±0.1	CV,IP			21.8	3466.2	B4
<b>IGR J16173-5023</b>	244.314	-50.386	3.3	0.7±0.1	< 0.3	?			7.9	3433.3	B4
PSR J1617-5055	244.339	-50.940	3.3	0.6±0.1	0.8±0.1	PSR			7.7	3415.0	burst
IGR J16185-5928	244.617	-59.473	3.4	0.8±0.1	1.0±0.2	AGN,NLSy1			8.5	2212.9	B5
IGR J16194-2810	244.877	-28.130	2.9	1.9±0.2	1.4±0.3	LMXB,Symb			10.6	712.7	B3
AX J161929-4945	244.894	-49.742	1.4	2.0±0.1	1.2±0.1	HMXB?,SFXT?			21.3	3384.6	B5
Sco X-1	244.980	-15.642	0.2	589.0±0.2	17.4±0.3	LMXB,Z,M			6314.2	768.1	B5
<b>IGR J16206-5253</b>	245.149	-52.883	4.6	< 0.2	< 0.3	?			5.1	3236.7	burst
IGR J16207-5129	245.188	-51.506	0.9	3.1±0.1	2.2±0.1	HMXB,S <sub>g</sub>			33.9	3267.8	B5
<b>IGR J16226-2759</b>	245.641	-27.995	4.8	< 0.5	< 0.7	?;T			5.1	750.2	R405B2
SWIFT J1626-6-5156	246.660	-51.937	1.7	0.4±0.1	< 0.3	HMXB,XP,T	Y	10.0±0.8	15.7	3233.5	burst
4U 1624-490	247.007	-49.205	0.6	4.0±0.1	0.5±0.1	LMXB,D			64.4	3409.9	B4
IGR J16283-4838	247.066	-48.660	1.2	1.2±0.1	0.6±0.1	HMXB?,NS?	Y	17.5±0.8	23.1	3286.5	burst
<b>IGR J16285-4630</b>	247.113	-46.507	4.8	< 0.2	< 0.3	?;T	Y	8.1±2.0	5.2	3373.7	S397B5
IGR J16287-5021	247.160	-50.375	3.1	0.7±0.1	< 0.3	HMXB?			8.5	3272.5	B4
IGR J16318-4848	247.949	-48.819	0.3	27.3±0.1	14.2±0.1	HMXB,S <sub>g</sub> ,Be			293.1	3445.6	B5
AX J1631.9-4752	248.007	-47.877	0.3	15.8±0.1	5.7±0.1	HMXB,XP,S <sub>g</sub> ,T			157.5	3259.4	B1

Table 3—Continued

Name <sup>a</sup>	RA	Dec	Err or <sup>b</sup>	F20-40 <sup>c</sup>	F40-100 <sup>c</sup>	Type <sup>d</sup>	Vari <sup>e</sup>	Peak flux <sup>f</sup>	Signif <sup>g</sup>	Exposure <sup>h</sup>	MapCode <sup>i</sup>
4U 1626-67	248.069	-67.463	0.5	16.6±0.2	1.9±0.4	LMXB,XP	YY	2.1±0.7	86.1	811.9	B4
<b>IGR J16327-4940</b>	248.172	-49.666	4.5	< 0.2	0.4±0.1	? ,T	Y	7.7±0.2	5.6	3319.3	R292B3
IGR J16328-4726 <sup>j</sup>	248.193	-47.440	0.8	2.9±0.1	2.3±0.1	?	Y	179.4±0.4	41.8	3193.4	R287B5
4U 1630-47	248.507	-47.397	0.2	23.8±0.1	20.4±0.1	LMXB,BHC,D,T	Y	477.7	3299.6	burst	
IGR J16351-5806	248.816	-58.088	2.6	1.1±0.1	1.2±0.2	AGN,Sy2	Y	10.4	2351.0	B3	
IGR J16358-4726	248.981	-47.427	0.7	1.2±0.1	0.8±0.1	LMXB?,XP,T,Sg?	Y	28.6±0.6	46.1	3122.5	burst
IGR J16377-6423	249.553	-64.362	3.3	1.0±0.2	< 0.6	Cluster?	?	8.1	1055.3	B4	
IGR J16385-2057	249.640	-20.909	4.8	0.8±0.2	0.7±0.3	AGN,NLSy1	?	5.5	1065.6	B3	
<b>IGR J16388+3557</b>	249.708	35.959	4.9	1.0±0.3	1.5±0.6	?	?	4.9	302.2	S338B5	
AX J163904-4642	249.774	-46.707	0.6	5.9±0.1	0.8±0.1	LMXB,XP,T	Y	66.8	3425.0	B4	
4U 1636-536	250.230	-53.753	0.3	27.4±0.1	15.8±0.2	LMXB,B,A	Y	280.1	2902.4	B5	
<b>IGR J16413-4046</b>	250.337	-40.781	4.5	0.4±0.1	0.5±0.2	?	?	5.2	3531.4	B2	
IGR J16418-4532	250.461	-45.542	0.7	4.7±0.1	1.1±0.1	LMXB,XP,SFXT?	Y	46.1	3349.8	B1	
<b>IGR J16424-2222</b>	250.605	-22.371	4.5	0.7±0.2	0.8±0.2	?	?	5.6	1358.3	B3	
IGR J16426+6336	250.649	65.608	3.9	2.2±0.6	< 1.9	AGN,NLSy1	Y	7.6±1.2	6.2	97.0	burst
<b>IGR J16443+0131</b>	251.080	1.524	5.2	1.0±0.3	< 1.0	?	?	5.1	313.4	B4	
<b>IGR J16447-5138</b>	251.178	-51.649	4.5	< 0.2	< 0.3	? ,T	Y	23.9±6.1	4.7	2942.8	burst
GX 340+0	251.447	-45.614	0.2	30.8±0.1	1.7±0.1	LMXB,Z	Y	478.3	3457.3	B4	
IGR J16465-4507	251.666	-45.121	1.7	1.4±0.1	0.7±0.1	LMXB,XP,SFXT?	Y	16.7	3537.4	S222B5	
IGR J16479-4514	251.990	-45.201	0.8	4.0±0.1	2.0±0.1	HMXB,SFXT	Y	42.7	3518.2	burst	
IGR J16482-3036	252.063	-30.587	1.3	2.1±0.1	2.4±0.2	AGN,Sy1	Y	22.3	2862.5	B3	
<b>IGR J16486-1323</b>	252.160	-13.399	4.5	< 0.5	< 0.7	? ,T	Y	5.5	778.2	burst	
IGR J16493-4348	252.359	-43.826	1.2	2.4±0.1	1.4±0.1	HMXB,Sg	Y	24.8	3738.6	B5	
IGR J16500-3307	252.489	-33.108	2.0	1.5±0.1	0.7±0.2	CV,IP	Y	13.4	3353.0	B1	
<b>SWIFT J 1650.5+0434</b>	252.647	4.595	4.4	1.4±0.3	1.2±0.6	AGN,Sy2	Y	5.2	286.9	burst	
ESO 138-1 <sup>j</sup>	253.045	-59.212	2.8	1.2±0.1	1.3±0.2	AGN,Sy2	Y	9.4	1755.6	B5	
NGC 6221 <sup>j</sup>	253.045	-59.212	2.8	1.2±0.1	1.3±0.2	AGN,Sy1/Sy2	Y	9.4	1755.6	B5	
<b>NGC 6240</b>	253.258	2.387	2.2	2.8±0.3	3.5±0.5	AGN,Sy2	Y	12.2	341.8	B5	
<b>Mrk 501</b>	253.488	39.753	2.6	3.1±0.3	2.1±0.6	AGN,BL Lac	Y	11.0	303.7	B5	
GRO J1655-40	253.498	-39.851	0.3	10.7±0.1	13.0±0.1	LMXB,BH,T,M	Y	220.6±0.9	323.9	4132.6	burst
<b>RXS J165443.5-191620</b>	253.704	-19.281	2.5	1.3±0.2	0.5±0.2	?	?	10.0	2150.0	B5	
<b>IGR J16560-4958</b>	253.989	-49.967	4.1	0.6±0.1	0.5±0.2	?	?	6.5	3029.4	burst	
IGR J16558-5203	254.043	-52.066	1.6	1.7±0.1	1.7±0.2	AGN,Sy1.2	Y	17.8	2571.0	B5	
SWIFT J1656.3-3302	254.086	-33.052	1.4	1.4±0.1	2.1±0.1	AGN,Blazar	Y	21.0	4057.5	burst	
Her X-1	254.458	35.336	0.2	96.0±0.3	15.0±0.5	LMXB,XP	Y	421.6	327.8	burst	
<b>IGR J16582-2937</b>	254.548	-29.626	4.6	0.4±0.1	< 0.3	? ,T	Y	5.4	3685.3	R172B5	
AX J1700.2-4220	255.083	-42.325	1.4	2.1±0.1	1.4±0.1	LMXB	Y	21.2	3426.2	B5	

Table 3—Continued

Name <sup>a</sup>	RA	Dec	Error <sup>b</sup>	F20-40 <sup>c</sup>	F40-100 <sup>c</sup>	Type <sup>d</sup>	Vari <sup>e</sup>	Peak flux <sup>f</sup>	Signif <sup>g</sup>	Exposure <sup>h</sup>	MapCode <sup>i</sup>
IGR J17008-6425	255.106	-64.403	5.0	< 0.5	0.9±0.4	?	Y	1.1±0.3	4.5	822.6	burst
OAO 1657-415	255.201	-41.658	0.2	70.9±0.1	38.5±0.1	HMXB,XP	Y	21.6±0.3	732.9	3924.6	B5
XTE J1701-462	255.245	-46.187	0.4	3.8±0.1	0.7±0.2	LMXB,B,T	Y	10.4±2.8	5.1	236.2	R340B5
<b>IGR J17028+2749</b>	255.700	27.823	4.9	< 0.8	1.5±0.7	? ,T	Y	133.7	3134.2	burst	
GX 339-4	255.705	-48.797	0.2	41.9±0.1	43.0±0.2	LMXB,BH,T,M	Y	600.3±0.8	890.1	2861.2	R525B5
4U 1700-377	255.987	-37.846	0.2	201.2±0.1	120.8±0.1	HMXB,Sg	YY	2321.8	5474.9	B5	
<b>IGR J17044-1844</b>	256.089	-18.735	4.6	< 0.3	0.6±0.2	? ,T	YY	4.9±1.2	5.4	2787.5	burst
GX 349+2	256.440	-36.426	0.2	44.7±0.1	1.1±0.1	LMXB,Z	YY	778.2	5542.5	B4	
4U 1702-429	256.559	-43.039	0.3	16.2±0.1	10.6±0.1	LMXB,B,A	YY	172.6	3748.0	B5	
IGR J17088-4008	257.203	-40.159	1.6	1.0±0.1	2.4±0.1	AXP	YY	17.2	4690.3	B3	
4U 1705-440	257.224	-44.104	0.3	21.0±0.1	8.8±0.2	LMXB,B,A	YY	238.8	3349.8	B4	
4U 1705-32	257.224	-32.319	0.8	3.1±0.1	2.8±0.1	LMXB,B	YY	39.0	5495.6	B5	
IGR J17091-3624	257.283	-36.407	0.4	4.6±0.1	6.0±0.1	LMXB?,BHC,T	Y	13.8±0.2	103.6	5422.1	burst
XTE J1709-267	257.381	-26.659	1.3	0.5±0.1	0.5±0.1	LMXB,B,T	Y	16.3±0.8	22.3	4772.1	burst
IGR J17098-3628	257.441	-36.463	0.5	3.7±0.1	3.9±0.1	LMXB?,BHC,T	Y	44.6±0.6	85.3	5326.5	burst
<b>IGR J17099-2418</b>	257.466	-24.302	3.4	0.6±0.1	< 0.3	? ,T	Y	1.5±0.3	7.6	3537.6	S285B5
XTE J1710-281	257.551	-28.138	0.9	2.9±0.1	2.8±0.1	LMXB,B,T	YY	38.4	5317.5	B3	
<b>IGR J17111+0611</b>	257.766	6.198	4.7	< 0.6	< 1.0	? ,T	YY	5.1	392.8	R603B2	
<b>RX J1713.7-3946</b>	257.953	-39.953	3.0	1.0±0.1	0.4±0.1	SNR	YY	9.9	4749.9	B1	
4U 1708-40	258.083	-40.861	1.6	1.0±0.1	0.5±0.1	LMXB,B,A	YY	17.6	4348.9	B4	
Oph Cluster	258.114	-23.356	0.7	4.9±0.1	1.0±0.1	Cluster	YY	55.3	4613.2	B4	
SAX J1712.6-3739	258.146	-37.647	0.7	4.4±0.1	3.7±0.1	LMXB,B,T	YY	55.6	5625.7	B5	
V2400 Oph	258.162	-24.258	0.9	3.5±0.1	1.0±0.1	CV,IP	YY	35.6	4453.6	B1	
XTE J1716-389	258.957	-38.837	2.9	0.6±0.1	0.6±0.1	HMXB,Sg?,T	Y	1.7±0.2	10.4	5190.4	S047B4
NGC 6300	259.242	-62.826	1.5	4.0±0.2	3.7±0.4	AGN,Sy2	YY	19.5	824.6	B5	
<b>IGR J17173-5855</b>	259.325	-58.930	5.0	0.4±0.2	< 0.5	? ,T	YY	1.6±0.3	4.9	1418.5	S047B1
MCG+08-31-041	259.760	49.017	4.7	2.4±0.8	6.2±1.3	AGN,Sy1	YY	5.5	72.5	B3	
IGR J17191-2821	259.808	-28.327	3.3	0.2±0.1	< 0.2	LMXB,B,T,A	YY	9.5±1.3	8.1	6947.0	burst
IGR J17196-1836	259.896	-18.606	4.8	< 0.2	< 0.3	? ,T	YY	4.2±2.1	5.2	3909.6	R303B1
IGR J17195-4100	259.908	-41.015	1.2	2.4±0.1	1.4±0.1	CV,IP	YY	24.3	4279.1	B5	
IGR J17198-3020	259.962	-30.342	3.8	0.4±0.1	0.4±0.1	? ,T	YY	6.7	6680.1	R229B5	
XTE J1720-318	259.998	-31.756	0.5	1.1±0.1	1.8±0.1	LMXB,BHC,T	YY	29.0±0.5	82.0	7088.6	burst
IGR J17200-3116	260.025	-31.288	0.9	2.4±0.1	1.2±0.1	HMXB,T	YY	34.2	7138.5	B4	
IGR J17204-3554	260.104	-35.888	2.2	0.7±0.1	1.3±0.1	AGN	YY	12.6	6360.3	B3	
<b>IGR J17219-1509</b>	260.482	-15.161	4.2	< 0.3	< 0.4	AGN?	YY	6.4±1.7	6.0	2409.0	R480B3
<b>IGR J17239-3143</b>	260.972	-31.721	4.9	< 0.1	< 0.2	? ,T	YY	4.7±0.9	5.1	7351.9	S534B1
EXO 1722-363	261.297	-36.284	0.4	9.5±0.1	2.8±0.1	HMXB,XP,Sg	YY	118.9	6546.1	B1	

Table 3—Continued

Name <sup>a</sup>	RA	Dec	Error <sup>b</sup>	F20-40 <sup>c</sup>	F40-100 <sup>c</sup>	Type <sup>d</sup>	Vari <sup>e</sup>	Peak flux <sup>f</sup>	Signif <sup>g</sup>	Exposure <sup>h</sup>	MapCode <sup>i</sup>
IGR J17254-3257	261.366	-32.964	1.0	1.9±0.1	1.9±0.1	LMXB,B	Y	11.6±1.5	29.6	7622.6	B5
IGR J17269-4737	261.694	-47.650	3.1	< 0.3	0.7±0.2	XB?,BHC,T	YY	2.8±1.2	9.4	2196.0	burst
<b>IGR J17276-0123</b>	261.888	-1.393	4.7	< 0.4	0.6±0.3	? ,T			5.3	1014.0	S163B4
GRS 1724-30	261.889	-30.805	0.3	18.4±0.1	14.7±0.1	LMXB,G,B,A			297.1	7883.1	B5
IGR J17285-2922	262.167	-29.364	2.2	< 0.1	< 0.2	XB?,T			12.2	7268.8	burst
<b>IGR J17299-4404</b>	262.486	-44.068	4.3	< 0.2	< 0.3	? ,T			5.8	2799.2	burst
IGR J17303-0601	262.592	-5.991	1.2	3.6±0.2	2.4±0.3	CV,IP			24.1	1450.0	B5
IGR J17314-2854	262.819	-28.904	3.4	< 0.1	< 0.2	?			7.7	7829.4	burst
GX 9+9	262.935	-16.963	0.3	12.3±0.1	< 0.3	LMXB,A			176.4	3487.0	B4
V2487 Oph	262.969	-19.217	2.9	0.5±0.1	0.9±0.1	CV,IP?			9.1	4562.3	B3
GX 354-0	262.991	-33.835	0.2	43.5±0.1	16.4±0.1	LMXB,B,A			685.9	7512.6	B4
GX 1+4	263.010	-24.748	0.2	53.1±0.1	41.7±0.1	LMXB,XP			869.1	6866.9	burst
IGR J17331-2406	263.306	-24.143	1.4	0.2±0.1	0.5±0.1	?			21.6	6961.9	burst
4U 1730-335	263.350	-33.388	0.4	4.4±0.1	2.1±0.1	LMXB,G,RB,T			116.1	7699.0	burst
IGR J17348-2045	263.737	-20.747	3.6	0.3±0.1	0.9±0.1	?			7.8	5419.2	burst
IGR J17354-3255	263.853	-32.939	1.4	1.4±0.1	1.0±0.1	HMXB?			20.6	7548.2	B5
<b>IGR J17353-3539</b>	263.863	-35.669	4.7	0.3±0.1	0.6±0.1	HMXB?			5.5	5957.9	burst
GRS 1734-294	264.370	-29.134	0.5	5.3±0.1	4.5±0.1	AGN,Sy1			91.1	8092.0	B5
IGR J17379-3747	264.466	-37.792	2.7	0.3±0.1	0.3±0.1	? ,T			5116.1	burst	
SLX 1755-269	264.571	-26.995	0.3	10.7±0.1	9.4±0.1	LMXB,B			179.2	7643.5	B5
4U 1755-444	264.742	-44.452	0.3	26.9±0.1	0.9±0.2	LMXB,B,A			310.4	2432.3	B4
XTE J1739-302	264.797	-30.344	0.8	1.3±0.1	0.8±0.1	HMXB,SFXT			43.9	8472.0	burst
AX J1739.3-2923	264.841	-29.390	4.5	0.3±0.1	0.4±0.1	?			6.6	8047.1	B3
IGR J17394-3007	264.861	-30.121	4.2	0.2±0.1	< 0.2	? ,T			6.0	8279.6	R408B4
<b>GRS 1736-297</b>	264.896	-29.743	2.0	0.4±0.1	0.6±0.1	HMXB,Be?			13.5	8004.7	burst
XTE J1739-285	264.989	-28.487	0.6	1.4±0.1	0.9±0.1	LMXB,B,T			14.5±0.3	63.4	8038.4
<b>AX J1740.2-2903</b>	265.074	-29.012	2.7	0.5±0.1	< 0.2	?			8.8	8488.0	B4
IGR J17404-3655	265.120	-36.934	2.3	1.1±0.1	0.8±0.1	LMXB?			12.5	5379.1	B1
SLX 1737-282	265.179	-28.291	0.6	4.0±0.1	3.9±0.1	LMXB,B			68.4	7766.8	B3
<b>IGR J17410-4156</b>	265.247	-41.934	4.7	< 0.2	0.5±0.2	?			6.2	3135.7	R105B4
<b>IGR J17413-1912</b>	265.317	-19.213	3.9	0.2±0.1	0.4±0.1	? ,T			7.6	5375.0	S478B3
<b>IGR J17413-2344</b>	265.318	-23.748	4.3	0.3±0.1	0.4±0.1	? ,T			5.4	7242.8	R489B1
IGR J17419-2802	265.459	-28.034	1.7	0.3±0.1	0.4±0.1	? ,T			16.3	7457.5	burst
2E 1739.1-1210	265.483	-12.206	1.8	1.7±0.1	1.7±0.2	AGN,Sy1.2			15.6	2458.5	B5
IGR J17426-0258	265.644	-2.965	4.5	< 0.3	< 0.5	? ,T			5.5	1679.7	R429B1
<b>IGR J17427-7319</b>	265.673	-73.329	4.5	1.5±0.4	< 1.5	?			5.5	197.9	burst
XTE J1743-363	265.754	-36.377	0.7	3.1±0.1	2.4±0.1	? ,SFXT?			7.8±0.2	5546.4	burst

Table 3—Continued

Name <sup>a</sup>	RA	Dec	Error <sup>b</sup>	F20-40 <sup>c</sup>	F40-100 <sup>c</sup>	Type <sup>d</sup>	Vari <sup>e</sup>	Peak flux <sup>f</sup>	Signif <sup>g</sup>	Exposure <sup>h</sup>	MapCode <sup>i</sup>
<b>IGR J17431-5945</b>	265.776	-59.765	4.8	< 0.5	< 0.7	? , T	Y	6.3±2.8	5.1	803.1	R050B4
1E 1740.7-2942	265.978	-29.745	0.2	29.8±0.1	36.7±0.1	LMXB,BHC,M	YY	2.7±0.3	13.1	557.3	8583.6
IGR J17445-2747	266.116	-27.766	2.2	< 0.1	0.3±0.1	?				7294.8	B3
IGR J17448-3232	266.199	-32.538	3.2	0.5±0.1	0.5±0.1	?			9.3	8185.5	B4
KS 1741-293	266.242	-29.337	0.5	4.3±0.1	3.5±0.1	LMXB,B,T			77.4	8516.5	S163B5
<b>GRS 1741.9-2853</b>	266.249	-28.919	0.7	2.9±0.1	1.8±0.1	LMXB,B,T			47.9	8628.5	B1GCF
IGR J17456-2901j	266.410	-29.021	0.5	5.5±0.1	3.3±0.1	?			91.6	8590.5	B1GCF
<b>IGR J17457-2858j</b>	266.428	-28.982	0.0	5.7±0.1	3.7±0.1	? , T			95.1	8588.7	B1GCF
<b>IGR J17459-2902j</b>	266.485	-29.043	0.0	4.8±0.1	2.9±0.1	? , T			79.1	8565.9	B1GCF
1A 1742-294j	266.523	-29.515	0.3	14.6±0.1	7.9±0.1	LMXB,B			245.2	8559.2	B5
IGR J17464-3213	266.565	-32.233	0.2	17.1±0.1	13.8±0.1	LMXB,BHC,T	Y	262.5±0.3	834.2	8231.0	burst
1E 1743.1-2843j	266.580	-28.735	0.5	5.1±0.1	2.2±0.1	LMXB?			83.8	8215.9	BIGCF
<b>IGR J17463-2854j</b>	266.587	-28.907	0.0	4.9±0.1	3.1±0.1	? , T			81.4	8456.3	BIGCF
<b>IGR J17467-2848j</b>	266.683	-28.805	0.0	4.6±0.1	2.4±0.1	? , T			76.7	8415.9	BIGCF
<b>IGR J17468-2902j</b>	266.690	-29.045	0.0	2.0±0.1	1.2±0.1	? , T			31.3	8437.9	BIGCF
SAX J1747.0-2853j	266.761	-28.883	0.5	3.3±0.1	2.0±0.1	LMXB,B,T	Y	19.0±0.2	82.3	8389.4	BIGCF
IGR J17473-2721	266.827	-27.346	1.7	0.2±0.1	0.5±0.1	LMXB,B,T	YY	3.8±0.3	16.0	7772.0	burst
IGR J17475-2822j	266.858	-28.396	0.9	2.2±0.1	1.8±0.1	mol cloud?			38.4	8231.9	B5
SLX 1744-299	266.858	-29.999	0.4	8.7±0.1	5.4±0.1	LMXB,B			147.0	8707.3	B5
IGR J17476-2253	266.892	-22.890	1.8	0.9±0.1	1.2±0.1	AGN,Sy1			15.5	7359.7	B3
GX 3+1	266.981	-26.565	0.3	10.6±0.1	1.0±0.1	LMXB,B,A			245.9	7246.7	B4
<b>IGR J17479-2807j</b>	266.982	-28.121	0.9	1.0±0.1	0.8±0.1	? , T			37.0	7886.9	B5
<b>IGR J17482-1020</b>	267.054	-10.336	4.6	< 0.2	< 0.4	? , T	YY	3.4±0.8	5.4	2446.5	R658B4
1A 1744-361	267.061	-36.130	1.1	0.7±0.1	0.9±0.1	LMXB,NS?,T	Y	16.8±0.7	26.4	5052.7	burst
<b>IGR J17488-2338</b>	267.197	-23.635	4.7	< 0.2	0.4±0.1	AGN?,T	YY	3.4±0.8	5.3	6226.2	burst
IGR J17488-3253	267.212	-32.905	0.9	2.0±0.1	2.6±0.1	AGN,Sy1			34.0	7838.9	B3
4U 1745-203	267.225	-20.364	1.2	0.4±0.1	0.9±0.1	LMXB,G,T	YY	18.4±0.9	24.3	5735.0	burst
AX J1749.1-2733	267.288	-27.546	1.2	1.6±0.1	1.3±0.1	HMXB,XP,B <sub>e</sub>			25.9	6990.6	burst
<b>IGR J17497-2821</b>	267.409	-28.357	0.3	3.0±0.1	3.6±0.1	LMXB,BHC,Symb?	YY	72.7±0.4	252.7	7714.8	burst
SLX 1746-331	267.458	-33.200	0.7	1.1±0.1	1.6±0.1	LMXB,BHC,T	Y	8.7±0.3	46.3	7704.1	burst
<b>IGR J17502-2858j</b>	267.549	-28.981	2.8	0.5±0.1	0.4±0.1	LMXB,B,T			9.5	8466.7	B4
4U 1746-370	267.559	-37.055	0.7	3.6±0.1	0.5±0.1	LMXB,G,B,A			53.4	4786.2	B4
IGR J17507-2647	267.665	-26.754	1.7	1.1±0.1	0.9±0.1	HMXB?			16.8	7491.0	B5
IGR J17507-2856j	267.692	-28.948	2.0	0.5±0.1	< 0.2	? , T	Y	2.1±0.2	13.9	8319.5	S222B5
GRS 1747-312	267.694	-31.275	1.2	1.6±0.1	1.3±0.1	LMXB,G,T			27.5	8346.2	burst
<b>XTE J1751-305</b>	267.804	-30.621	1.3	< 0.1	< 0.2	LMXB,XP	YY	22.4±1.2	22.7	8429.7	burst
IGR J17513-2011	267.812	-20.221	1.5	1.1±0.1	1.7±0.1	AGN,Sy1.9			18.5	5979.9	B5

Table 3—Continued

Name <sup>a</sup>	RA	Dec	Error <sup>b</sup>	F20-40 <sup>c</sup>	F40-100 <sup>c</sup>	Type <sup>d</sup>	Vari <sup>e</sup>	Peak flux <sup>f</sup>	Sigfig <sup>g</sup>	Exposure <sup>h</sup>	MapCode <sup>i</sup>	
<b>IGR J17520-6018</b>	268.009	-60.305	5.0	1.0±0.3	1.6±0.4	AGN?	Y	1.4±0.5	5.0	591.9	B3	
<b>1RXS J175252.0-053210</b>	268.203	-5.539	4.2	0.7±0.1	0.5±0.2	AGN?	Y	74.1±0.2	6.0	2260.5	B5	
SWIFT J1753.5-0127	268.369	-1.456	0.2	51.6±0.1	68.7±0.2	LMXB,BHC,T	Y	579.9	1885.6	burst		
<b>IGR J17536-2339</b>	268.373	-23.642	5.2	< 0.1	< 0.2	HMXB?		4.5	7270.2	burst		
IGR J17544-2619	268.593	-26.324	0.9	0.8±0.1	0.2±0.1	HMXB,SFXT	Y	33.7±1.0	37.2	8112.6	burst	
<b>IGR J17585-3057</b>	269.572	-30.966	3.0	0.6±0.1	0.6±0.1	?		8.7	7418.4	burst		
IGR J17586-2129	269.656	-21.356	2.6	0.8±0.1	0.5±0.1	LMXB?		10.4	6757.4	B5		
IGR J17597-2201	269.941	-22.032	0.5	4.8±0.1	4.2±0.1	LMXB,B,D		76.8	6580.6	burst		
GX 5-1	270.284	-25.081	0.2	49.7±0.1	3.2±0.1	LMXB,Z		1120.8	7218.8	B4		
GRS 1758-258	270.302	-25.747	0.2	56.3±0.1	74.1±0.1	LMXB,BHC,M		1103.8	7473.9	B3		
<b>IGR J18014+0202</b>	270.338	2.040	4.7	< 0.3	< 0.5	?T	Y	7.3±1.8	5.1	1664.1	R243B2	
GX 9+1	270.387	-20.533	0.2	16.2±0.1	0.3±0.1	LMXB,A		349.9	5634.6	B4		
IGR J18027-1455	270.689	-14.907	1.3	2.1±0.1	2.4±0.2	AGN,Sy1		22.9	3657.5	B5		
SAX J1802.7-201	270.690	-20.277	0.6	5.3±0.1	1.7±0.1	HMXB,XP,T,Be/Sg?		65.1	5856.7	B1		
IGR J18048-1455	271.184	-14.960	2.6	1.1±0.1	0.7±0.1	LMXB		10.3	3696.5	B1		
XTE J1807-294	271.749	-29.404	0.9	0.2±0.1	< 0.2	LMXB,XP,T	YY	15.8±0.5	35.5	7322.6	burst	
<b>IGR J18079-0921</b>	271.970	-9.360	4.8	< 0.2	< 0.3	?T	Y	3.5±0.8	5.1	3091.7	R485B4	
SGR 1806-20	272.167	-20.416	0.7	3.1±0.1	4.0±0.1	SGR		46.6	5816.6	B3		
<b>XTE J1810-189</b>	272.583	-19.092	3.0	< 0.2	< 0.3	XB,NS,T		8.7	5519.0	R660B5		
PSR J1811-1926	272.854	-19.425	2.2	0.8±0.1	1.1±0.1	SNR,PSR,PWN?		12.1	5799.2	B5		
<b>IGR J18129-0649</b>	273.224	-6.829	4.1	0.4±0.1	< 0.3	AGN?		5.6	2954.7	burst		
IGR J18134-1636	273.362	-16.621	3.7	0.5±0.1	0.6±0.1	?		7.4	4607.3	B5		
IGR J18135-1751	273.398	-17.847	1.6	1.3±0.1	1.7±0.1	SNR,PWN,PSR		17.6	5031.6	B5		
<b>IGR J18136-2739</b>	273.400	-27.650	4.1	< 0.2	< 0.2	?T	YY	2.5±0.4	6.0	6822.7	burst	
GX 13+1	273.626	-17.157	0.3	12.4±0.1	2.2±0.1	LMXB,B,A		194.7	4526.4	B4		
M 1812-12	273.774	-12.099	0.3	25.5±0.1	25.8±0.2	LMXB,B		284.0	3315.1	B5		
GX 17+2	274.006	-14.036	0.2	61.8±0.1	3.7±0.2	LMXB,B,Z		875.8	3456.7	B4		
IGR J18173-2509	274.348	-25.154	1.7	1.4±0.1	0.4±0.1	CW,IP		16.5	5744.5	B1		
<b>IGR J18175-1530</b>	274.426	-15.472	4.7	0.2±0.1	< 0.3	?T		6.1	3960.2	burst		
XTE J1817-330	274.429	-33.024	0.3	6.0±0.1	4.2±0.1	LMXB,BHC,T	Y	74.1±0.4	223.3	5949.8	burst	
<b>XTE J1818-245</b>	274.609	-24.536	1.0	0.9±0.1	0.4±0.1	LMXB,BHC,T	Y	17.9±0.6	30.2	4504.5	burst	
SAX J1818.6-1703	274.649	-17.044	0.6	1.5±0.1	1.2±0.1	HMXB,SFXT	Y	122.0±2.2	58.7	4355.7		
AX J1820.5-1434	275.123	-14.569	1.0	1.8±0.1	1.4±0.2	HMXB,XP,Be	Y	11.4±0.4	33.2	3565.0	burst	
IGR J18214-1318	275.335	-13.319	1.8	1.6±0.1	1.3±0.2	HMXB,T		15.8	3243.9	B5		
<b>IGR J18222-7312</b>	275.557	-73.208	5.3	< 0.9	< 1.7	?T	YY	13.2±2.9	4.7	150.8	S100B1	
4U 1820-303	275.917	-30.362	0.2	34.5±0.1	2.2±0.1	LMXB,G,B,A		587.8	5484.9	B4		
IGR J18244-5622	276.064	-56.360	3.9	1.9±0.3	1.3±0.5	AGN,Sy2		6.1	399.1	B5		

Table 3—Continued

Name <sup>a</sup>	RA	Dec	Error <sup>b</sup>	F20-40 <sup>c</sup>	F40-100 <sup>c</sup>	Type <sup>d</sup>	Vari <sup>e</sup>	Peak flux <sup>f</sup>	Signif <sup>g</sup>	Exposure <sup>h</sup>	MapCode <sup>i</sup>	
IGR J18246-1425	276.107	-14.441	3.3	0.8±0.1	0.4±0.2	?_XP?			8.0	3528.9	B1	
IGR J18249-3243	276.206	-32.708	3.4	0.6±0.1	0.6±0.1	AGN,Sy1			8.2	4831.2	burst	
4U 1822-000	276.343	-0.015	1.2	1.6±0.1	< 0.4	LMXB			24.7	2813.5	B4	
IGR J18256-1035	276.442	-10.579	3.4	0.8±0.1	< 0.3	?			7.8	3294.7	B1	
3A 1822-371	276.447	-37.107	0.3	31.3±0.1	3.5±0.1	LMXB,P,M			326.8	4043.9	B4	
IGR J18259-0706	276.500	-7.158	3.0	0.8±0.1	0.8±0.2	AGN,Sy1			8.7	3130.7	B5	
LS5039	276.525	-14.847	2.5	0.8±0.1	1.4±0.2	HMXB,NS,M			10.6	3696.0	B3	
<b>IGR J18280-2939</b>	276.991	-29.644	3.2	0.3±0.1	< 0.3	?_T			3.1±0.4	5118.5	burst	
<b>IGR J18284-0343</b>	277.075	-3.723	3.4	< 0.2	< 0.3	?_T			3.5±0.6	7.7	2960.1	burst
GS 1826-24	277.366	-23.799	0.2	82.6±0.1	66.7±0.1	LMXB,B			1031.0	5219.8	B5	
<b>XTE J1829-098</b>	277.439	-9.897	4.0	0.3±0.1	< 0.3	HMXB,XP,T			8.8±1.5	6.1	S283B4	
AX J183039-1002	277.647	-10.056	3.4	0.7±0.1	0.5±0.2	AGN?			7.6	3166.1	B5	
IGR J18308-1232	277.694	-12.515	3.5	0.6±0.1	0.7±0.2	CV,IP			7.0	3265.0	B5	
<b>IGR J18311-3337</b>	277.810	-33.597	2.5	0.7±0.1	1.2±0.1	AGN			9.6	4156.4	B3	
<b>AX J1832-3-0840</b>	278.071	-8.690	4.6	0.5±0.1	< 0.3	CV			5.4	3090.6	B4	
IGR J18325-0756	278.118	-7.949	1.0	2.0±0.1	1.1±0.2	HMXB?,T			32.2	3090.6	burst	
SNR 021.5-00.9	278.392	-10.568	1.0	3.0±0.1	3.1±0.2	SNR,PWN			33.6	3132.1	B5	
PKS 1830-211	278.415	-21.063	1.0	2.4±0.1	3.2±0.1	AGN,QSO/Blazar			30.5	4258.2	B3	
3C382	278.695	32.703	4.5	4.2±0.9	2.9±1.3	AGN,Sy1			5.3	71.6	B1	
RX J1832-33	278.933	-32.990	0.4	10.0±0.1	9.9±0.1	LMXB,G,B,T			113.8	4204.6	B5	
<b>IGR J18363-0124</b>	279.068	-1.414	4.7	< 0.2	< 0.3	?_T			5.4±1.8	5.3	R174B4	
<b>IGR J18371+2634</b>	279.265	26.570	5.2	1.8±0.5	< 1.5	?			4.5	226.6	B5	
AX J1838.0-0655	279.505	-6.918	1.2	1.9±0.1	2.7±0.2	SNR,PSR,PWN?			24.0	2989.6	B3	
ESO 103-35	279.553	-65.409	3.5	4.3±0.7	5.2±1.2	AGN,Sy2			7.4	77.0	B3	
Ser X-1	279.991	5.033	0.3	11.2±0.1	0.4±0.2	LMXB,B			154.5	2762.2	B4	
AX J1841.0-0536	280.256	-5.587	1.5	1.1±0.1	0.9±0.2	HMXB,XP,SFXT			19.6	2984.1	burst	
Kes 73	280.335	-4.943	1.0	2.2±0.1	4.0±0.2	SNR,AXP			30.3	3007.6	B3	
3C 390.3	280.563	79.766	2.1	3.0±0.3	4.1±0.5	AGN,Sy1			13.7	307.9	B3	
IGR J18450-0435	281.254	-4.588	1.8	1.5±0.1	1.0±0.2	HMXB,SFXT?			14.9	2925.5	B5	
GS 1843+009	281.404	0.865	0.6	3.6±0.1	2.9±0.2	HMXB,XP,Be,T			65.5	3160.8	burst	
<b>IGR J18457+0244</b>	281.420	2.745	4.3	0.5±0.1	0.7±0.1	?			5.8	3403.9	B3	
<b>IGR J18464-0223</b>	281.594	-2.394	4.1	0.5±0.1	0.6±0.2	?			6.0	2979.8	B4	
PSR J1846-0258	281.602	-2.984	1.4	1.7±0.1	2.2±0.2	SNR,PSR,PWN			19.9	2980.7	B3	
<b>IGR J18482+0049</b>	282.043	0.829	4.4	0.4±0.1	0.3±0.2	?			5.8	3318.2	B5	
IGR J18483-0311	282.071	-3.171	0.7	4.4±0.1	2.8±0.2	HMXB,SFXT			47.3	2899.6	burst	
3A 1845-024	282.082	-2.434	2.2	0.6±0.1	0.6±0.2	HMXB,XP,Be?,T			12.5	2887.2	B5	
IGR J18485-0047	282.106	-0.780	2.8	0.9±0.1	0.9±0.2	?			9.2	2977.0	B5	

Table 3—Continued

Name <sup>a</sup>	RA	Dec	Error <sup>b</sup>	F20-40 <sup>c</sup>	F40-100 <sup>c</sup>	Type <sup>d</sup>	Vari <sup>e</sup>	Peak flux <sup>f</sup>	Signif <sup>g</sup>	Exposure <sup>h</sup>	MapCode <sup>i</sup>
IGR J18490-0000	282.268	-0.012	2.2	1.0±0.1	1.5±0.2	PWN?,PSR?	YY	4.0±0.9	12.4	3104.2	B3
<b>IGR J18498+1608</b>	282.454	16.139	4.1	<0.3	0.5±0.2	?;T			5.9	2046.6	burst
4U 1850-087	283.265	-8.705	0.7	5.2±0.1	4.4±0.2	LMXB,G,B			49.7	2391.2	B5
<b>IGR J18532+0416</b>	283.288	4.267	4.5	0.3±0.1	0.6±0.1	?			5.6	3700.8	B3
<b>IGR J18538-0102</b>	283.459	-1.034	4.8	0.4±0.1	0.4±0.2	?			5.2	2955.5	B5
IGR J18539+0727	283.493	7.470	0.8	0.5±0.1	0.7±0.1	XB,BHC,T	YY	18.3±0.6	40.7	3393.8	burst
V1223 Sgr	283.761	-31.161	0.7	6.8±0.1	3.1±0.2	CV,IP			53.8	2358.5	B5
XTE J1855-026	283.878	-2.608	0.4	11.0±0.1	6.8±0.2	HMXB,XP,T			106.7	2808.2	B5
2E 1853.7+1534	283.995	15.619	2.1	1.5±0.1	1.3±0.2	AGN,Sy1.2			14.0	2271.2	B5
XTE J1858+034	284.680	3.440	0.3	10.1±0.1	1.2±0.1	HMXB,XP,Be?;T	Y	96.3±0.3	298.6	3546.3	burst
HETE J1900.1-2455	285.037	-24.921	0.3	15.4±0.1	13.1±0.2	LMXB,XP,B	Y	34.5±0.2	172.0	1601.8	burst
<b>IGR J19015+0421</b>	285.370	4.364	4.9	<0.2	<0.3	?;T			5.1	3701.2	R291B5
XTE J1901+014	285.420	1.448	1.0	2.7±0.1	2.4±0.1	HMXB,SFXT?;T			31.1	3331.3	B5
4U 1901+03	285.914	3.204	0.2	25.9±0.1	3.1±0.1	HMXB,XP,T	Y	106.5±0.2	651.3	3612.7	burst
IGR J19048-1240	286.196	-12.671	4.3	0.4±0.1	<0.5	?			5.8	1467.5	R365B1
<b>IGR J19060-0055</b>	286.500	-0.920	4.7	<0.2	<0.3	?;T			5.2	2381.2	R301B1
<b>IGR J19071-2858</b>	286.783	-28.974	4.2	0.3±0.1	<0.5	?;T			4.9	1512.0	S047B1
SGR 1900+14	286.836	9.312	2.0	1.1±0.1	0.8±0.1	SGR			13.7	3579.6	burst
<b>IGR J19077-3925</b>	286.911	-39.427	3.6	0.6±0.1	1.1±0.2	AGN			6.6	1698.6	B3
<b>IGR J19079+0942</b>	286.985	9.711	4.7	<0.2	<0.3	?;T			5.2	3469.0	R060B3
XTE J1908+094	287.223	9.384	0.8	1.0±0.1	1.2±0.1	LMXB,BHC,T	Y	10.2±0.3	41.0	3598.8	burst
4U 1907+097	287.409	9.829	0.3	16.8±0.1	1.4±0.1	HMXB,XP,T			201.9	3564.0	B4
AX J1910.7+0917	287.665	9.271	3.1	0.4±0.1	0.6±0.1	?			8.3	3698.2	burst
4U 1909+07	287.701	7.597	0.3	14.1±0.1	7.9±0.1	HMXB,XP			166.2	3694.0	B5
Aql X-1	287.817	0.584	0.3	12.0±0.1	10.3±0.2	LMXB,B,A,T	Y	76.5±0.4	202.1	2604.6	burst
<b>IGR J19113+1533</b>	287.821	15.553	4.0	<0.2	<0.3	?;T			6.4	2389.5	R193B5
<b>IGR J19118-1707</b>	287.938	-17.129	4.7	0.8±0.2	<0.6	AGN?			4.8	981.4	B5
<b>IGR J19118+1125</b>	287.943	11.418	4.9	<0.2	<0.3	?;T			5.1	3450.1	R307B4
SS 433	287.955	4.984	0.4	8.9±0.1	4.3±0.1	HMXB,M			106.0	3561.9	burst
IGR J19140+0951	288.514	9.887	0.4	9.0±0.1	5.5±0.1	HMXB,S <sub>g</sub>			105.6	3502.0	B5
GRS 1915+105	288.798	10.944	0.2	284.4±0.1	123.2±0.1	LMXB,BH,T,M			3243.8	3613.1	B4
4U 1916-053	289.702	-5.237	0.6	9.4±0.1	5.4±0.2	LMXB,B,D			66.9	1476.2	B5
<b>PKS 1916-300</b>	289.888	-29.986	3.5	1.0±0.2	<0.5	AGN?			7.6	1222.8	B5
SWIFT J1922.7-1716	290.634	-17.285	1.4	2.4±0.2	1.4±0.4	LMXB?;NS?,BH,C?	Y	7.5±0.4	21.4	694.3	burst
<b>IGR J19239+1546</b>	290.976	15.778	4.7	<0.2	<0.3	?;T	YY	4.0±0.8	5.3	2661.5	R176B1
1RXS J192450.8-291437	291.227	-29.227	3.9	0.9±0.2	0.8±0.3	AGN,BL Lac/Blazar			6.6	1091.6	burst
<b>IGR J19251-5137</b>	291.276	-51.618	5.3	0.6±0.3	1.4±0.5	?			4.6	438.6	B5

Table 3—Continued

Name <sup>a</sup>	RA	Dec	Error <sup>b</sup>	F20-40 <sup>c</sup>	F40-100 <sup>c</sup>	Type <sup>d</sup>	Vari <sup>e</sup>	Peak flux <sup>f</sup>	Signif <sup>g</sup>	Exposure <sup>h</sup>	MapCode <sup>i</sup>
<b>IGR J19254-3901</b>	291.358	-39.029	4.1	< 0.3	< 0.5	?;T	YY	6.5±1.7	6.1	1521.8	S047B3
<b>IGR J19254+1047</b>	291.359	10.796	4.5	0.3±0.1	< 0.3	?;T	Y	3.2±0.7	5.6	3142.0	R423B4
IGR J19267+1325	291.662	13.405	3.3	0.7±0.1	0.4±0.2	CV,IP			8.1	2963.9	B5
<b>IGR J19294-1746</b>	292.341	-17.782	5.2	0.6±0.3	1.3±0.4	?;T	Y	3.8±1.1	4.8	512.6	burst
<b>IGR J19295-0919</b>	292.376	-9.319	5.2	0.7±0.2	1.2±0.3	?			4.6	737.2	B3
<b>SWIFT J1930.5+3414</b>	292.528	34.160	4.1	1.3±0.2	0.8±0.3	AGN,Sy1.5-1.8	Y	1.7±0.3	5.7	736.7	B1
<b>IGR J19311+1708</b>	292.786	17.139	4.5	< 0.3	< 0.4	?;T	YY	1.4±0.5	5.5	2212.1	S067B4
<b>IGR J19313-0359</b>	292.831	-3.991	4.8	< 0.4	< 0.5	?;T	Y	5.4±1.8	5.2	1131.9	R064B3
<b>QSO B1933-400</b>	294.294	-39.932	4.4	0.5±0.1	1.0±0.2	AGN,QSO/Blazar	Y	0.6±0.1	5.9	1430.1	burst
<b>IGR J19375-0012</b>	294.363	-0.233	5.3	< 0.3	< 0.5	?;T	YY	3.2±0.8	4.7	1492.4	S373B1
IGR J19378-0617	294.409	-6.218	4.2	1.3±0.2	0.9±0.3	AGN,NLSy1			6.1	727.0	B3
<b>IGR J19386-4653</b>	294.653	-46.886	4.5	< 0.4	< 0.6	?;T	YY	7.0±1.4	6.0	917.0	burst
V1432 Aql	295.056	-10.424	2.5	3.1±0.3	1.6±0.5	CV,P,asynch			11.3	429.7	B5
IGR J19405-3016	295.074	-30.272	3.5	1.2±0.2	< 0.6	AGN,Sy1.2			7.5	1014.7	burst
NGC 6814	295.669	-10.322	2.4	3.0±0.3	3.6±0.5	AGN,Sy1.5			11.3	380.2	burst
IGR J19443+2117	296.039	21.307	4.4	0.8±0.2	0.6±0.3	AGN?			5.7	1180.8	burst
<b>IGR J19475+0049</b>	296.873	0.829	4.7	0.7±0.2	< 0.5	?;T	Y	5.4±1.4	5.2	1164.0	R367B4
KS 1947+300	297.394	30.207	0.6	6.7±0.2	5.1±0.3	HMXB,XP,T	Y	21.1±0.4	57.4	989.5	burst
<b>3C 403</b>	298.083	2.514	3.4	0.8±0.2	1.5±0.3	AGN,Sy2			7.3	1089.6	B3
<b>IGR J19536+5307</b>	298.392	53.127	4.5	< 0.7	< 1.0	?;T	YY	3.0±1.0	5.6	449.6	R510B4
<b>IGR J19552+0044</b>	298.796	0.745	4.3	1.1±0.2	< 0.7	?			5.8	845.1	B5
4U 1954+31	298.927	32.095	0.6	10.7±0.2	4.6±0.3	LMXB,NS,Symb	Y	16.1±0.2	70.2	1047.9	burst
Cyg X-1	299.590	35.199	0.2	747.1±0.2	877.5±0.2	HMXB,BH,M			5744.1	1786.5	B5
Cyg A	299.867	40.738	1.1	4.8±0.2	5.0±0.3	AGN,Sy2			26.1	1014.2	B5
SWIFT J2000.6+3210	300.076	32.197	1.9	2.2±0.2	2.0±0.3	HMXB,Be			14.3	1264.9	B4
ESO 399-20	301.735	-34.548	4.7	0.7±0.2	1.3±0.3	AGN,Sy1			5.5	932.4	B3
<b>IGR J20146+5112</b>	303.656	51.209	4.9	0.7±0.2	1.0±0.3	?			4.9	867.8	B2
<b>IGR J20155+3827</b>	303.875	38.450	4.2	< 0.3	< 0.5	?;T	YY	5.8±1.8	5.9	1314.2	R233B4
IGR J20186+4043	304.683	40.706	3.2	1.3±0.2	1.4±0.2	AGN,Sy2			1202.1	burst	
<b>IGR J20231+5302</b>	305.774	53.036	4.5	< 0.4	< 0.6	?;T	YY	2.6±0.8	5.2	1082.5	burst
IGR J20286+2544	307.122	25.751	2.9	2.0±0.3	3.3±0.4	AGN,Sy2			9.0	469.4	B3
<b>IGR J20293+5647</b>	307.322	56.795	4.9	< 0.4	< 0.7	?;T	Y	8.9±2.5	5.1	942.1	S081B4
EXO 2030+375	308.056	37.630	0.2	69.0±0.2	33.9±0.2	HMXB,XP,Be,T	Y	859.9±0.9	1437.2	1248.7	burst
Cyg X-3	308.106	40.955	0.2	171.0±0.2	70.8±0.2	HMXB,M			1244.5	1303.5	B4
4C 74.26	310.561	75.126	3.7	2.9±0.5	2.2±0.9	AGN,QSO			6.8	124.0	B5
<b>IGR J20450+7530</b>	311.257	75.503	4.7	2.6±0.5	< 1.7	?			5.5	125.4	B1
<b>IGR J20526-4320</b>	313.161	-43.345	4.2	0.9±0.4	< 1.4	?;T	Y	11.1±2.3	5.9	262.6	R258B5

Table 3—Continued

Name <sup>a</sup>	RA	Dec	Error <sup>b</sup>	F20-40 <sup>c</sup>	F40-100 <sup>c</sup>	Type <sup>d</sup>	Vari <sup>e</sup>	Peak flux <sup>f</sup>	Sig/ff <sup>g</sup>	Exposure <sup>h</sup>	MapCode <sup>i</sup>
<b>IGR J20552-2846</b>	313.794	-28.776	5.1	2.1±0.9	< 3.0	? <sub>T</sub>	Y	7.5±3.2	4.7	68.4	B4
<b>IGR J20569+4940</b>	314.171	49.684	4.2	0.8±0.1	0.4±0.2	AGN?			6.5	1851.9	B4
<b>IGR J20594+3625</b>	314.858	36.432	4.5	< 0.4	< 0.5	? <sub>T</sub>			5.5	1107.4	R185B4
<b>IGR J21012+4538</b>	315.311	45.649	4.2	0.7±0.1	0.5±0.2	?			5.7	1796.4	B4
SAX J2103.5+4545	315.896	45.749	0.3	14.4±0.1	8.0±0.2	HMXB,XP,B <sub>e</sub> ,T	Y	138.5±1.0	154.2	1893.7	R553B5
<b>1RXS J211336.1+542226</b>	318.470	54.371	4.3	0.7±0.1	0.6±0.2	?			6.1	1881.2	B5
S52116+81	318.724	82.090	3.9	1.9±0.4	< 1.4	AGN,Sy1			6.1	201.6	B5
IGR J21178+5139	319.466	51.638	2.8	0.8±0.1	1.3±0.2	AGN?			9.5	2135.9	B3
<b>IGR J21188+4901</b>	319.699	49.017	4.3	< 0.2	< 0.4	?			5.8	2163.3	S047B3
<b>1RXS J211928.4+333259</b>	319.898	33.551	5.0	0.8±0.2	1.0±0.3	AGN			5.0	697.3	B2
V2069 Cyg	320.928	42.326	3.4	1.0±0.1	0.5±0.2	CV,IP			7.4	1648.8	B1
IGR J21247+5058	321.162	50.970	0.5	7.1±0.1	7.7±0.2	AGN,Sy1			72.3	2217.2	B5
<b>IGR J21268+6203</b>	321.692	62.062	4.4	< 0.3	< 0.5	AGN?	YY	2.1±0.7	5.9	1421.8	burst
SWIFT J2127.4+5654	321.923	56.935	1.6	2.4±0.1	1.4±0.2	AGN,NLSy1			19.4	1781.0	B5
<b>IGR J21286+4956</b>	322.143	49.945	4.9	< 0.2	< 0.4	? <sub>T</sub>	YY	3.4±1.1	5.1	2277.7	R443B1
<b>4U 2129+12</b>	322.490	12.161	2.4	4.8±0.5	5.0±0.9	LMXB,G,B <sup>?,D</sup>			11.5	105.5	B5
<b>IGR J21319+3619</b>	322.981	36.331	5.0	< 0.4	< 0.6	?			5.0	969.5	S51.1B3
IGR J21335+5105	323.433	51.120	1.1	3.0±0.1	1.5±0.2	CV,IP			26.8	2207.4	B5
IGR J21347+4737j	323.626	47.614	3.4	0.4±0.1	< 0.4	HMXB,B <sub>e</sub>	Y	2.1±0.3	7.7	2159.7	burst
RX J2135.9+4728j	323.985	47.487	2.6	1.0±0.1	1.1±0.2	AGN,Sy2			10.7	2126.3	B5
<b>1RXS J213944.3+595016</b>	324.928	59.827	4.5	0.6±0.1	0.6±0.2	?			5.5	1772.1	burst
SS Cyg	325.697	43.578	1.2	3.2±0.1	1.8±0.2	CV,DN			23.8	1674.3	B5
<b>IGR J21441+4640</b>	326.017	46.681	4.9	< 0.2	0.4±0.2	? <sub>T</sub>	YY	2.8±0.8	5.0	2009.5	S1.92B4
Cyg X-2	326.168	38.319	0.3	25.9±0.2	2.6±0.3	LMXB,B,Z			228.2	1076.6	B4
<b>PKS 2149-306</b>	327.980	-30.446	5.1	1.2±0.3	1.7±0.6	AGN,QSO/Blazar			4.9	243.1	B5
<b>IGR J21523-2240</b>	328.078	-22.678	3.9	1.5±0.5	< 1.9	? <sub>T</sub>	Y	7.0±1.3	6.4	105.3	burst
<b>IGR J21565+5948</b>	329.126	59.815	4.9	0.3±0.1	0.8±0.2	?			5.1	2058.3	B5
Mrk 520	330.126	10.603	4.3	2.1±0.5	2.7±0.9	AGN,Sy1.9			5.8	111.1	B5
<b>IGR J22014+6034</b>	330.361	60.567	5.4	< 0.2	< 0.4	?			4.6	2169.0	S047B4
NGC 7172	330.500	-31.877	1.6	4.5±0.3	4.8±0.6	AGN,Sy2			17.7	245.5	B5
BL Lac	330.667	42.293	2.9	1.3±0.2	1.5±0.3	AGN,BL Lac			9.2	1191.0	B5
4U 2206+543	331.985	54.514	0.5	8.8±0.1	6.5±0.2	HMXB,B <sub>e</sub>			81.6	2116.4	B5
<b>IGR J22127+1358</b>	333.183	13.968	4.3	2.1±0.4	1.7±0.7	AGN?	Y	4.9±1.0	6.5	160.5	burst
FO Aqr	334.497	-8.360	4.3	3.3±0.8	< 2.8	CV,IP			6.1	54.1	B4
IGR J22234-4116	335.850	-41.260	4.1	0.9±0.4	3.5±0.8	?			5.4	135.7	B2
<b>IGR J22253+5046</b>	336.325	50.777	4.8	< 0.3	< 0.5	?			5.2	1866.0	S463B5
IGR J22292+6647	337.299	66.757	4.1	0.6±0.1	0.7±0.2	AGN,Sy1			6.1	2270.3	B5

Table 3—Continued

Name <sup>a</sup>	RA	Dec	Error <sup>b</sup>	F20-40 <sup>c</sup>	F40-100 <sup>c</sup>	Type <sup>d</sup>	Vari <sup>e</sup>	Peak flux <sup>f</sup>	Signif <sup>g</sup>	Exposure <sup>h</sup>	MapCode <sup>i</sup>
NGC 7314	338.896	-26.072	4.1	1.5±0.5	2.0±0.8	AGN,Sy1.9	Y	3.1±0.7	5.6	153.7	B5
<b>4C 452</b>	341.393	39.724	5.0	1.6±0.5	1.9±0.8	AGN,Sy2			4.6	211.5	B5
<b>IGR J22517+2218</b>	342.919	22.292	3.9	1.3±0.4	2.3±0.7	AGN,QSO/Blazar	Y	2.0±0.5	6.5	191.3	burst
<b>3C 454.3</b>	343.489	16.149	1.0	9.4±0.4	12.8±0.7	AGN,QSO/Blazar			30.8	183.2	B3
QSO B2251-178	343.539	-17.581	2.7	3.7±0.6	4.1±1.0	AGN,Sy1			9.0	99.1	B4
<b>AO Psc</b>	343.825	-3.162	4.8	2.1±0.5	< 1.7	CV,P			4.9	108.7	B4
<b>IGR J22560+5152</b>	344.004	51.882	4.6	< 0.3	< 0.5	?T	YY	2.3±0.7	5.7	2039.9	R511B3
NGC 7465	345.532	15.944	4.9	1.1±0.4	1.9±0.7	AGN,Sy2			4.7	182.4	burst
<b>IGR J23029+4535</b>	345.717	45.595	4.3	< 0.5	< 0.9	?T			5.8	712.5	R557B1
NGC 7469 <sup>j</sup>	345.819	8.892	4.2	3.2±0.5	2.2±0.9	AGN,Sy1			6.6	113.1	B1
MCG-02-58-022	346.181	-8.676	4.0	2.7±0.4	2.4±0.7	AGN,Sy1.5			6.7	139.5	B5
<b>IGR J23070+2203</b>	346.740	22.063	4.9	1.4±0.4	< 1.3	?			4.9	202.3	burst
NGC 7582	349.591	-42.399	4.8	3.7±1.1	< 3.7	AGN,Sy2			5.2	52.5	S373B5
<b>IGR J23206+6431</b>	350.202	64.539	3.9	0.5±0.1	< 0.3	AGN,Sy1			6.2	3356.2	burst
Cas A	350.848	58.813	0.7	4.0±0.1	2.4±0.1	SNR			51.7	3348.1	B4
IGR J23308+7120	352.650	71.363	4.6	0.7±0.1	< 0.4	AGN,Sy2			5.7	1995.1	B1
<b>IGR J23494+5941</b>	357.341	59.699	4.9	< 0.2	< 0.3	?T			5.0	3602.2	R051B1
<b>IGR J23504+1653</b>	357.607	16.887	4.5	4.4±0.9	< 3.0	?T	Y	5.3±1.3	5.5	44.0	B1
IGR J23524+5842	358.053	58.761	3.3	0.5±0.1	0.9±0.1	AGN,Sy2			8.4	3498.2	B3
<b>IGR J23558-1047</b>	358.939	-10.788	4.5	2.8±0.8	4.3±1.4	?			5.2	57.1	burst

<sup>a</sup>Names in bold face indicate new detections since third catalog

<sup>b</sup>Position errors expressed as radius of 90% confidence circle in arcminutes

<sup>c</sup>Time-averaged flux expressed in units of mCrab; appropriate conversion factors are: (20-40 keV) 10 mCrab =  $7.57 \times 10^{-11}$  erg cm<sup>-2</sup> s<sup>-1</sup> =  $1.71 \times 10^{-3}$  ph cm<sup>-2</sup> s<sup>-1</sup>; (40-100 keV) 10 mCrab =  $9.42 \times 10^{-11}$  erg cm<sup>-2</sup> s<sup>-1</sup> =  $9.67 \times 10^{-4}$  ph cm<sup>-2</sup> s<sup>-1</sup>

<sup>d</sup>Source type classifications: A=Atoll source (neutron star); AGN=Active galactic nuclei; AXp=Anomalous X-ray pulsar; B=Burster (neutron star); Be=B-type emission-line star; BH=Black hole (confirmed mass evaluation); BHC=Black hole candidate; BL=broad line; Cluster=Cluster of galaxies; CV=Cataclysmic variable; D=Dipping source; DN=Dwarf Nova; G=Globalular Cluster X-ray source; GRB=Gamma-Ray Burst; HMXB=High-mass X-ray binary; IP=Intermediate Polar; LMXB=Low-mass X-ray binary; M=Microquasar; Mol Cloud=Molecular cloud; NL=narrow line; NS=Neutron Star; P=Polar; PSR=Radio pulsar; PWN=Pulsar wind nebula; QSO=Quasar; RG=Radio galaxy; SFXT=Supergiant Fast X-ray Transient; SG=Supergiant; SGR=Soft gamma-ray repeater; SNR=Supernova remnant; Sy=Seyfert galaxy; Symb=Symbiotic star; T=Transient source; XB=Galactic X-ray binary; XBONG=X-ray bright, optically normal galaxy; XP=X-ray pulsar; Z=Z-type source (neutron star)

<sup>e</sup>Variability indicator, see Section 4 for details

<sup>f</sup>Peak flux in 20-40 keV band, measured during largest detected outburst, see section 4 for details

<sup>g</sup>Maximum significance in a single map; see mapcode column to identify map with maximum significance.

<sup>h</sup>Corrected on-source exposure (ksec)

<sup>i</sup>Map with maximum significance: B1=20-40 keV, B2=30-60 keV, B3=20-100 keV, B4=17-30 keV, B5=18-60 keV; a prefix of RXXX indicates detection in revolution XXX, SXXX indicates detection in revolution sequence beginning at revolution XXX, ST=Starling data. Burst indicates that significance and position were obtained from a data subset defined by *bursticity* analysis (see section 2.4). B1GCF indicates derived from fitting of Galactic Center (see section 3)

<sup>j</sup>Blended source. Position determined by simultaneous fitting is reliable, but other measured values (flux, significance) may be contaminated by nearby